

# tribology in industry



## contents



INTRODUCTION	Instead of Introduction: ITC In Session Meeting at Esslingen; Tribology 2000-Plus - A Great Success . . . . .	119
RESEARCH	C. PANDAZARAS, G. PETROPOULOS: On The Relationship Between Surface Waviness and Roughness Parameters in Turning/ Assessment of Hydrodynamically Lubricated Journal Bearings Performance . . . . .	121
	M. KUZINOVSKI, P. CICHOSZ , H. ZEBROWSKI, Z. STAMBOLISKA: Research of The Correlation Between The Two- dimensional and Three-dimensional Roughness of The Machined Surfaces at Increased Speed of Turning . . . . .	133
	C. GHEORGHIES, M. SIMIONOV: Study on Tribomodel of The Damage Process in The Diesel Engine Cylinder Liners . . . . .	139
NEWS	. . . . .	148
BOOKS AND JOURNALS	. . . . .	149
SCIENTIFIC MEETINGS	. . . . .	150

## ITC In Session Meeting at Esslingen

The fourteenth meeting of the ITC In Session took place on Monday 10th January 2000 at the Technische Akademie Esslingen.

It was attended by Vice Presidents and representatives of Vice Presidents and Corresponding Members from 26 Member Groups or Societies.

Discussions took place on a number of subjects.

A change of the Statutes was agreed by a resolution that was passed, es-

tablishing a sub-committee comprising of a member of each of the societies where congresses had taken place to consider the suitability of the next vacant event.

For 2005 only one application, jointly from STLE and ASME had been received. The meeting instructed the sub-committee to obtain full particulars and make their recommendation at the next ITC In Session meeting on 2nd September 2001, which will be held the evening prior to the 2<sup>nd</sup>

WTC in Vienna at a venue to be notified.

**Professor Franek** presented a video giving a review of the preparation of the 2nd World Tribology Congress in Vienna on 3<sup>th</sup>-7<sup>th</sup> September 2001 and answered questions. A second leaflet was produced, a copy of which is attached.

The proceedings ended by thanking Professor Dr-Ing Bartz for making available the facilities of this meeting at his Academy.

## Tribology 2000-Plus - A Great Success

827 participants attended the first Tribology Colloquium of the millennium at Esslingen, Germany. They came from 41 countries and presented 247 papers covering a wide range of facets of tribology, in particular subjects relating to nano tribology and applications, present and future, and applications of tribology to computers in general were much in evidence.

As at previous colloquia Tribology 2000-Plus was excellently organised. It was well spread amongst the nine parallel sessions, even more so than on most previous occasions.

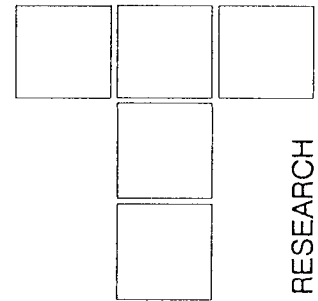
In addition to being the first tribology conference of the millennium and as already reported above, ITC President, Professor H Peter Jost, was presented with the world's first Honorary Doctorate of the millennium at the beginning of the conference by repre-

sentatives of the V.A. Belyi Metal-Polymer Research Institute of the Academy of Sciences of Belarus. Another first for tribology.

The Proceedings started with eight Plenary lectures:

- Recent Developments and Future Needs of the International Tribology Council H Peter Jost - International Tribology Council, London, UK

- Trends and Directions for Tribology Research and Development in the Coming Years W.O. Winer, E.C. Gwwaltney - Georgia Institute of Technology, Atlanta, USA
- The World Lubricants Market - Current Situation and Outlook M. Fuchs - Fuchs Petrolub AG, Mannheim, Germany
- Future Importance of Base Oils in Lubricants
- T Mang - Fuchs Petrolub AG, Mannheim, Germany
- Additives for the Next Millennium
- S.A. Si Biase - The Lubrizol Corporation, Wickcliffe, USA
- Automotive Lubricants for the Next Millennium
- S. Korcek. J. Sorab, M.D. Johnson, R.K. Jensen - Ford Research Laboratory, Dearborn, USA
- Tribology in Magnetic Recording Technology
- F.E. Talke - University of California, San Diego, USA
- Developments of Tribological Materials for the Next Millenium E. Santner- BAM, Berlin, Germany



C. PANDAZARAS, G. PETROPOULOS

# On The Relationship Between Surface Waviness and Roughness Parameters in Turning/Assessment of Hydrodynamically Lubricated Journal Bearings Performance

*The evaluation and analysis of waviness of technological surfaces is usually neglected, although it affects in many cases the surface tribological behaviour especially of machine elements like shafts and bushes. In the first part of this paper, the relationship between waviness and roughness of turned surfaces is sought in order to establish relevant laws or trends. On the basis of experiments carried out in four different lathe designations of different dynamic characteristics and the necessary surface texture measurements as well as corelevant statistical analysis it is indicated that:*

*Circumferential waviness is greater than axial waviness and greater also than circumferential roughness and very good correlation appears between roughness CLA value and waviness amplitude parameters leading to the formulation of exponential regression models. These results feed a mathematical model of hydrodynamic lubrication in finite journal bearings. In the proposed model the influence of the directional irregularities of the finite journal-bearing surface performance is considered. The well-known Reynolds equation of hydrodynamic lubrication for a Newtonian, isoviscous and incompressible fluid is applied under its general stochastic form (average Reynolds equation). The equilibrium equation is solved numerically by using a finite difference approximation scheme for a steady state condition.*

*Keywords: multi parameter surface characterization, surface waviness, machining processes, turning*

## 1. INTRODUCTION

The problem of technological surface texture control has been by far considered to be of paramount importance in design and manufacture of machine components. The main surface topography features are roughness and waviness. Many research contributions have been reported on roughness, as it constitutes a significant machinability parameter [22], [23], [10], [24].

On the other hand, waviness is usually overlooked though it plays a considerable role in the surface tribological behaviour, as in the hydrodynamic lubrication of journal bearings. Waviness strongly depends on the outputs of the machine tool system (vibration, eccentricity of workpiece or tool and others) and sometimes is regarded as a symptom of the aforementioned system condition: failures, worn or damaged parts etc. Hence, waviness characteristics may considerably vary with the dynamic characteristics of the system designation [35]. It is questionable if a part of waviness is correlated to the machining process performed and its parameters employed (Figure 1).

From the standpoint of machine elements tribologist recent studies over the last years [11], [12], [27] showed that the important problem of bearing surface waviness requires more investigations to be carried out, concerning waviness geometrical pattern and its effects on the bearing performance characteristics.

From the standpoint of machine elements tribologist recent studies over the last years [11], [12], [27] showed that the important problem of bearing surface waviness requires more investigations to be carried out, concerning waviness geometrical pattern and its effects on the bearing performance characteristics.

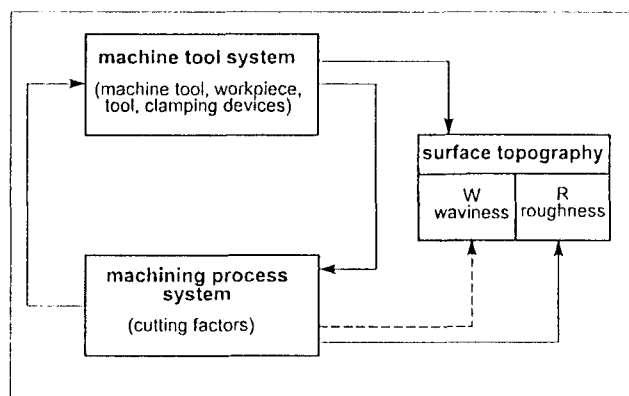


Fig. 1 Dependence of surface texture on machining process and machine tool systems

C. PANDAZARAS, G. PETROPOULOS  
Department of Mechanical and Industrial Engineering,  
University of Thessaly,  
383 34 Volos, Greece

Although, the results given by Rasheed compared with those obtained through simulation for realistic journal-bearing configurations (use of previous version of three-dimensional hydrodynamic lubrication code developed by the authors of this paper) [19] indicate that it is practically very difficult to draw conclusions due to specific reasons (low equivalent waviness circumferential number, big eccentricity ratio, big R/L ratio and others).

The present study is aimed at the assessment of hydrodynamic lubrication performance of turned journal bearings or shafts.

The first part of the present study is aimed at the investigation of the interrelationship of selected waviness parameters and roughness of turned surfaces under a combination of machining conditions and for different machine tool systems (lathe designations) regarding their dynamic characteristics. Also, related comparisons are made between the tested surface patterns in the axial and circumferential direction.

The foregoing results are introduced as inputs to a numerical model for the journal bearing functional performance, which is presented in the second part, in order to calculate essential tribological magnitudes as: journal center coordinates, minimum fluid film thickness, shaft and bearing friction forces (or moments).

## 2. EXPERIMENTAL

### 2.1. Equipment

The mode of turning followed was quasi steady state external longitudinal cylindrical turning. The necessary experiments were carried in four test lathe designations (A, B, C and D) of different static and dynamic stiffness (Table 1).

Table 1: Lathe designations characteristics

Lathe configuration	Nominal Power	Maximum distance between centers	Swing over bed
A	7.5 kw	1250 mm	195 mm
B	6.6 kw	2000 mm	250 mm
C*	7.5 kw	1250 mm	195 mm
D*	6.6 kw	2000 mm	250 mm

Designations C\* and D\* correspond to lathes A and B with a dynamometer mounted on their tables instead of their tool posts in order to alter the dynamic characteristics of the relevant lathe system.

High precision lathe A was in an excellent operational condition and fair precision lathe B was brand new.

Surface roughness and waviness measurements were undertaken by a profilometer setting  $0.8\text{ mm}$  as the cut-off length and  $5 \times 0.8\text{ mm}$  the evaluation length. Two skidless pick-ups were used: a common type pick-up for axial

measurements and a side pick-up for circumferential measurements. The selected waviness parameters were:

$W_a$ ,  $W_b$ ,  $W_z$ ,  $W_p$ ,  $W_{DelQ}$ ,  $W_{sk}$ ,  $W_{ku}$  and  $W_{sm}$  [26], which directly correspond to roughness parameters:

$R_a$ : central line average

$R_t$ : maximum peak to valley height in the evaluation length

$R_z$ : average of all  $R_{ti}$  values in the evaluation length

$R_p$ : maximum height above the central line

$R_{DelQ}$ : quadratic mean of all local slopes

$R_{sk}$ : skewness of the amplitude distribution curve

$R_{ku}$ : kurtosis of the amplitude distribution curve

$R_{sm}$ : mean spacing between profile peaks at the mean line

The multi parameter surface pattern analysis was conducted via software Talyprof.

### 2.2. Cutting tool-workpiece

The cutting tool, always sharp, was a sintered carbide P10 mounted on a standardized tool holder of the following combined geometry:

rake angle:  $\gamma = +6^\circ$

clearance angle:  $\alpha = 11^\circ$

inclination angle:  $\lambda_s = 0^\circ$

primary approach angle:  $\kappa = 75^\circ$

tool nose radius:  $r_e = 0.8\text{ mm}$

The workpieces-specimens were from plain carbon steel Ck 60 in the form of bars of  $50\text{ mm}$  diameter and of  $250\text{ mm}$  length.

No cutting fluid was used in the experiments.

### 2.3. Specimens preparation-cutting conditions

All specimens were clamped in both centers of the lathes.

Cutting conditions: depth of cut  $a = 0.5\text{ mm}$ , feed rate  $s$  ( $0.08 - 0.60$ )  $\text{mm rev}^{-1}$  and cutting speed  $v$  ( $100, 150$  and  $210$ )  $\text{m min}^{-1}$ .

In each machined specimen 40 surface texture measurements were conducted cited at random axially and circumferentially, respectively (sample size 40).

## 3. RESULTS AND DISCUSSION

### 3.1. Ratios of waviness to roughness (Amplitude parameters)

In Table 2 are listed relative magnitude ratios between mean values of waviness and roughness in both axial and circumferential directions.

It is obvious that waviness is much less than roughness in the axial direction, while the opposite appears in the

circumferential direction. An explanation for these findings can be that in the circumferential direction only process roughness occurs, which in steady state cutting is much lower than kinematic roughness, that is imparted in the axial direction. In this way, the effect of waviness is more pronounced in circumferential patterns.

Table 2: Waviness and roughness magnitude ratios

AXIAL $W_{ia}/R_{ia}$	CIRCUMFERENTIAL $W_{ic}/R_{ic}$	COMBINED $W_{ic}/W_{ia}$
$W_{aa}/R_{aa} = 0.103$	$W_{ac}/R_{ac} = 3.82$	$W_{ac}/W_{aa} = 2.158$
$W_{ia}/R_{ia} = 0.104$	$W_{ic}/R_{ic} = 1.39$	$W_{ic}/W_{ia} = 2.090$
$W_{za}/R_{za} = 0.045$	$W_{zc}/R_{zc} = 1.34$	$W_{zc}/W_{za} = 2.430$
$W_{pa}/R_{pa} = 0.104$	$W_{pc}/R_{pc} = 1.80$	$W_{pc}/W_{pa} = 1.230$

On the other hand, circumferential waviness is greater than axial waviness, something that can be attributed to the fact that circumferential direction is more sensitive to out of roundness errors caused by the machine tool system.

### 3.2. Characteristics in length of waviness

Examination of waviness characteristics in length reveals that in very low and low feed rates waviness has a random shape (Fig. 2a and 2b). On the contrary, in high feed rates it is almost harmonic (Fig. 2c). This fact may be attributed to increased rotational eccentricity of the workpiece due to increase of cutting force. The run-out wavelength is equal to the corresponding feed rate value.

Concerning the waviness mean spacing  $W_{sm}$  it appears to take high values in the range of medium and low feed rates, whereas at high feed rates it approaches feed marks wavelength values. Consequently, correlation between waviness and roughness mean spacings exists only for large feed rate values (Table 3).

Table 3: Waviness mean spacing  $W_{sm}$  against feed rate

s [mm.rev <sup>-1</sup> ]	$W_{sm}$ [μm] v=100 m/min	$W_{sm}$ [μm] v=150 m/min	$W_{sm}$ [μm] v=210 m/min
0.08	1583	2105	1845
0.10	1214	1431	1660
0.16	1147	974	1347
0.20	1003	901	1014
0.24	1062	926	1005
0.32	1113	1058	1446
0.40	431	560	424
0.50	550	544	532
0.60	671	669	646

### 3.3. Regression analysis models of waviness against roughness

Surface pattern in the axial direction in turning, which is the direction of cutting, is more documented and inter-

esting from the standpoint of manufacturing. Also, as  $R_a$  is the most popular roughness parameter the analysis is limited to the relationship between  $R_a$  and the selected waviness parameters in the axial direction.

Representative results in test lathe designation B are listed in Table 4. It is apparent that the formulated regression models show almost excellent correlation coefficients  $r$  between  $R_a$  and  $W_a, W_b, W_z, W_{DelQ}$ , while the statistical parameters  $W_{sk}$  and  $W_{ku}$  appear uncorrelated. Also, the reproducibility of the results was high enough for each lathe designation, as presented in Table 5.

Table 4: Connection of waviness parameters to  $R_a$  roughness in lathe designation B

Parameter	Cutting speed (m/min)	$b_0$	$b_1$	$r^2$	$r$
$W_a$	100	0.66	0.11	0.980	0.988
	150	0.28	0.16	0.960	0.980
	210	0.34	0.15	0.980	0.999
$W_t$	100	2.89	0.11	0.994	0.997
	150	1.14	0.17	0.972	0.986
	210	1.66	0.14	0.994	0.997
$W_z$	100	1.31	0.12	0.980	0.998
	150	0.50	0.20	0.980	0.990
	210	1.09	0.15	0.988	0.998
$W_p$	100	1.15	0.11	0.998	0.999
	150	0.66	0.17	0.964	0.982
	210	0.79	0.14	0.994	0.997
$W_{DelQ}$	100	0.57	0.09	0.990	0.995
	150	0.23	0.15	0.982	0.991
	210	0.30	0.13	0.998	0.999
$W_{sk}$	100	Uncorrelated			
	150				
	210				
$W_{ku}$	100	Poor Correlation			
	150				
	210				

In Table 6 generalized models are shown, that is for all four lathe designations exhibiting correlation coefficients varying from excellent to very good for the waviness parameters considered.

All models follow a positive exponential law:

$$[Y = b_0 \cdot \exp(b_1 \cdot X)].$$

According to these results it is concluded that waviness may be related to the same causes that affect roughness directly or indirectly via cutting factors like feed rate and cutting speed. Of course, the formulated regression models are far from being universal, as they possess more qualitative than quantitative character. Surface waviness

prediction regarding both the machining system and the machine tool system constitutes an ultimate goal needing further research.

Table 5: Indicative case of replication for waviness parameter  $W_a$  ( $v=210 \text{ m.min}^{-1}$ )

Feed rate $s$ [mm.rev <sup>-1</sup> ]	First test $W_a$ [ $\mu\text{m}$ ]	Replicated test $W_a$ [ $\mu\text{m}$ ]
0.08	0.578	0.445
0.10	0.306	0.417
0.16	0.395	0.340
0.20	0.365	0.325
0.24	0.483	0.401
0.32	0.483	0.610
0.40	2.630	2.470
0.50	8.000	8.11
0.60	32.80	32.60

Table 6: Association of waviness parameters with  $R_a$  roughness for all four lathe configurations. Generalized model.

Parameter	Cutting speed (m/min)	$b_0$	$b_1$	$r^2$	$r$
$W_a$	100	0.50	0.14	0.976	0.988
	150	0.22	0.21	0.956	0.978
	210	0.25	0.22	0.980	0.990
$W_t$	100	2.44	0.12	0.954	0.977
	150	1.11	0.22	0.958	0.979
	210	0.90	0.25	0.976	0.998
$W_z$	100	1.21	0.17	0.996	0.991
	150	0.51	0.24	0.980	0.990
	210	0.60	0.24	0.988	0.994
$W_p$	100	1.14	0.12	0.960	0.980
	150	0.60	0.18	0.962	0.981
	210	0.58	0.22	0.992	0.996
$W_{\text{DelQ}}$	100	0.52	0.16	0.982	0.991
	150	0.24	0.20	0.976	0.988
	210	0.29	0.21	0.988	0.994

#### 4. MODELLING OF ROUGH AND WAVY JOURNAL-BEARING HYDRODYNAMIC LUBRICATION

It seems that the aforementioned theoretical models investigating into the effect of surface irregularities, sometimes make unrealistic assumptions about waviness pattern in bearings and liners both axially and circumferentially. It must be noted that this fact is eventually a result of the relatively small size of meshes for the Rey-

nolds equation numerical resolution. In the circumferential direction a mesh size of approximately 40 gives the possibility to represent journal-bearing cross-section by using 90 points. This value of points population could be considered sufficient for waviness numbers below 10 under the hypothesis that one wave is represented by at least 9 points. Also axial waviness numbers larger than 10 demand a relatively dense grid of the bearing face. This density is not possible to be obtained with axial mesh's size larger than the axial wave length. However, in special cases the axial waviness could be partially neglected by using a waviness number smaller than 10, when the circumferential waviness effect is able to generate load support, which is not destroyed by the axial waviness effect on hydrodynamic load support mechanism of the lubricated contact.

In other cases contacts between the tribosystem technological surfaces occur and the proposed calculation code does not provide realistic results.

The present model was developed in order to simulate the partial hydrodynamic regime. This simulation concerns especially the limited contact area around the minimum lubricant fluid film. This area is not fully hydrodynamically lubricated because of roughness presence. The computer programme takes into consideration measured waviness and roughness magnitudes, as well as more realistic assumptions for journal-bearing configurations: R/L ratio 1, normal mean radial clearance value, amplitude of waviness form and waviness numbers. Contact between rough and wavy surfaces is assumed not to exist.

#### 4.1. The shaft-bearing hydrodynamic friction code

##### 4.1.1. Basic assumptions

This three-dimensional code takes into account the following parameters:

- ▶ Macro topography of the bearing (bush), as well as micro topography, axially and circumferentially due to the real shape of the machined journal bearings and shafts (lemon bearing, half lemon bearing, multilobe bearing. Offset-halves journal bearing known as displaced bearing [29-31], pericycloid bearing, spiral bearing, presence of circumferential, axial or combined waviness form in bearing liner [27]).
- ▶ Dynamic-alternating load (harmonic or not [1], [13], [30]).

In the present work, the basic assumptions made (additional to the Full Reynolds equation assumptions) concerning lubricating contact geometry, shaft-bearing relative motion and lubrication characteristics in a shaft-bearing combination are as follows:

## Kinematics - Geometry

The axis of journal and bush are always parallel and the cross-section perpendicular to them (zero tilt). The shaft equivalent cross section configuration is perfectly circular. There is no deformation of the shaft-bearing system under hydrodynamic pressure. The bearing is floating. The load is applied through the bearing.

## Lubrication

The oil film has sufficient thickness for the hydrodynamic equation to be valid (full average Reynolds equation) and the lubricating gap is completely filled with the lubricant.

Lubricant viscosity remains constant during the system operation (Newtonian isoviscous fluid). The lubricant is incompressible and the flow in the gap of finite length bearing is laminar.

## 4.2. Input-output parameters

Input Shaft geometry - diameter, Bearing (hole) geometry - diameter and length (total axial, normal to motion), Bearing macrotopography represented by axial and circumferential mean waviness values and their lengths as well as microtopography given by Gaussian profile characteristics represented by axial and circumferential r.m.s ( $\sigma$ ) values, Lubricant viscosity, Superficial film shear stress characteristics, Shaft rotation speed, Shaft - Bearing load function.

Output Oil film thickness - Journal center path, Hydrodynamic pressure, Friction forces, Friction coefficient and Power losses.

## 4.3. Principle of the model

The purpose of the model [13-17] is to calculate the load  $W_H$  supported by the hydrodynamic fluid lubricant film for given conditions even in the partial lubrication regime ( $h/\sigma_{po} < 3$ ).

Then the friction force (or moment)  $F_H$  (or  $M_H$ ) is calculated as the sum of the hydrodynamic oil film shearing forces (or moments), the squeeze term is introduced in the Reynolds equation.

The local value of the fluid lubricant thickness  $h_L$  can be determined by the following formula [17]:

$$h_L = h' + \delta_1 + \delta_2, \text{ where}$$

$h'$  is the nominal fluid lubricant film thickness determined as the local distance between the profiles reference lines or surfaces

$$\delta_i = w_i + \zeta_i$$

$\zeta_1$  and  $\zeta_2$  the surfaces points altitudes measured from their reference lines or surfaces. They take negative values where they represent surface peaks. The distribu-

tion functions of those populations are generally non Gaussian and their standard deviations are  $\sigma_{po1}$  and  $\sigma_{po2}$  respectively ( $po$  is related to the profile points populations). A composite roughness could be used in order to transform the problem into a simplified equivalent one, concerning contact between a composite rough surface and a smooth one. Both surfaces configurations are represented by their reference lines or surfaces. The composite surface point's altitudes will be  $\zeta = \zeta_1 + \zeta_2$  and its standard deviation  $\sigma_{po}^2 = \sigma_{po1}^2 + \sigma_{po2}^2$ .

$w_1$  and  $w_2$  the surfaces waviness measured from their reference lines or surfaces. Their values are negative where they represent surface hills. A composite waviness could also be used in order to transform the problem into a simplified equivalent one, regarding contact between a synthetic wave surface and a smooth one. The composite surface waviness will be  $w = w_1 + w_2$ . Generally when  $h/3\sigma_{po} > 1$ , it is admitted that microtopography irregularities effect does not exist.

Thus the apparent fluid lubricant film thickness becomes:

$$h = h' + w_1 + w_2 = h' + w \text{ and the local fluid lubricant thickness } h_L \text{ can be determined as } h_L = h + \delta$$

The cross section of the equivalent bearing operating with smooth shaft is characterized by its coordinates  $x(I,J)$ ,  $y(I,J)$  related to the smooth equivalent bearing center, where  $I$  is the circumferential index and  $J$  the longitudinal index.

Assuming a sinusoidal wave with 9 points, these coordinates become:

$$\begin{aligned} x(I,J) &= (D/2)\sin\theta_R + W_{AC}\sin\theta_C \sin\theta_R + W_{AL}\sin\theta_L \sin\theta_R \\ y(I,J) &= (D/2)\cos\theta_R + W_{AC}\sin\theta_C \cos\theta_R + W_{AL}\sin\theta_L \cos\theta_R \\ z(I,J) &= (J-1)W_{SmL}/8 \end{aligned}$$

$$\theta_C = 2\pi(I-1)/8$$

$$\theta_R = 2\pi(I-1)/(8n_{wC})$$

$$\theta_L = 2\pi(J-1)/8$$

$$I_{max} = 8n_{wC} + 1$$

$$J_{max} = 8n_{wL} + 1$$

$$n_{wC} = \pi D/W_{SmC} = \theta_C/\theta_R$$

$$n_{wL} = L/W_{SmL}$$

$n_{wC}$  and  $n_{wL}$  are the circumferential and the axial waviness numbers respectively.

The hydrodynamic oil film is calculated for a given separation of shaft - bearing surfaces. An iterative procedure is then carried out to calculate the value of the oil film thickness that yields the equilibrium between the contact forces and the load acting on the shaft - bearing system.

The hydrodynamic film is calculated with use of the most general stochastic form of the well known full Reynolds equation [3-4] introduced by Tzeng and Seidal [34] in dimensional or dimensionless form, in polar or rectangular coordinates for the developed surfaces, by adopting the half-Sommerfeld (Gümbel) conditions with  $p=0$  in

the specified cavitation position. This equation in dimensional form can be written as follows by using a Cartesian coordinate system in order to study the simple geometry of shaft and bush opened up:

$$\frac{\partial}{\partial x} \left( \Phi_x \frac{h^3}{12 \cdot n} \frac{\partial p}{\partial x} \right) + \frac{\partial}{\partial z} \left( \Phi_z \frac{h^3}{12 \cdot n} \frac{\partial p}{\partial z} \right) = \frac{U}{2} \frac{\partial h_T}{\partial x} + \frac{U}{2} \sigma_{po} \frac{\partial \Phi_s}{\partial x} + \frac{\partial h_T}{\partial t}$$

where:  $h$  macrogeometrical fluid lubricant film thickness  
 $h_T$  stochastic separation distance of surfaces calculated from  $h$  and roughness parameters  
 $n$  absolute lubricant viscosity  
 $p$  mean local hydrodynamic pressure  
 $U$  shaft surface speed, shear velocity  
 $\Phi_x, \Phi_z, \Phi_s$  pressure-shear flow factors reported by Patir and Cheng [20], [21], depending upon surface roughness, its anisotropy and local nominal oil film thickness [32-33].

By using Rohde [28] formula concerning flow factors and assuming the polynomial distribution function for roughness  $f(\delta) = (35/32) \cdot (c^2 - \delta^2) / c^7$  this equation is solved numerically by using Nystrom formula in the finite difference iterative method (Gauss-Seidal) for a mesh 1 mm maximum in  $x$  and 0.5 mm maximum in  $z$  direction [19].

The active part of the bearing is meshed at least in 200x80 elements.  $H$  is the node oil film thickness matrix defined from the real shape of the bearing, the shape of the shaft and the eccentricity between the shaft and the bearing.  $P$  finite difference grid nodes hydrodynamic pressure matrix is calculated by solving the Reynolds equation. The equivalent hydrodynamic force resulting by the computed hydrodynamic pressure must be equal and opposite to the applied bearing-shaft load.

For dynamically loaded journal bearing tribosystem calculation should start for a zero squeeze term action. Thereafter, for any subsequent time interval, the film thickness at the end of the previous time interval is known.

When the pressure equations have been satisfied, the pressure field is used to obtain flow characteristics and the next step is to calculate hydrodynamic friction forces by determining the sum  $F_H$  of all the elemental friction components acting on each element, given by the following expression (in this case this force is acting on the bearing surface):

$$F_H = \iint_A (\tau_{Hi} + \tau_{Hii}) dA$$

$$\tau_{Hi} = n \cdot U / h [h < 1/h_T > - \Phi_{fs}] - \Phi_{fp} \cdot h / 2 \cdot dp/dx$$

$$\tau_{Hii} = Vr_1 [(\Phi_{fp} \cdot h - h_T) \cdot dp/dx + 2 \cdot n \cdot U / h \Phi_{fs}]$$

Where:

$h$  - macrogeometrical fluid lubricant film thickness (compliance)  
 $h_T$  - stochastic separation distance of surfaces calculated from  $h$  and roughness parameters, local film thickness  
 $n$  - lubricant absolute (dynamic) viscosity  
 $p$  - mean local (nodal) hydrodynamic pressure  
 $U$  - shaft speed, shear velocity  
 $\Phi_{fs}, \Phi_{fp}$  shear stress factors [20], [27] depending upon surface roughness, its distribution function, its directional properties which characterize anisotropy and the local nominal oil film thickness  
 $\Phi_{fs} = Vr_1 \Phi_{fs}(h/\sigma, \gamma_1) - Vr_2 \Phi_{fs}(h/\sigma, \gamma_2)$   
 $\gamma_i$  surface pattern parameter, surface anisotropy index, ratio of  $x$  and  $z$  0.5 correlation lengths. Every 0.5 correlation length is defined as the length at which the profile correlation function reduces to 50% of its value at  $\lambda=0$ . Purely transversal, isotropic and longitudinal roughness patterns correspond to  $\gamma=0, 1, \infty$  (values respectively). The proposed  $\Phi$  functions are given generally for  $h > \sigma$ .  $\Phi_x, \Phi_z, \Phi_s$  are zero for  $h/\sigma \rightarrow \infty$  ( $\sigma = \sigma_{po}$ ).  
 $\delta_i$  - surface local altitude, measured from the mean reference surface.  
 $w_i$  - surface wave, measured from the mean reference surface.  
 $f_{po}(\delta)$  - measured probability density function of points altitudes population by using Fisher - Pearson analysis method  
 $i = 1$  for the liner,  $i = 2$  for the shaft  
 $\sigma_{oi}$  - standard deviations of the points altitudes measured distribution function  
 $\sigma_{po}$  - standard deviations of the composite measured distribution function

A nominal surface of contact

$$V_{ri} = \sigma_{poi}^2 / \sigma_{po}^2$$

$$\langle 1/h_T \rangle = \int_{-\infty}^{+\infty} \frac{f_{po}(\sigma) d\sigma}{(h+\delta)} \quad \text{and} \quad h_T = \int_{-h}^{+\infty} (h-\delta) f_{po}(\delta) d\delta$$

The constant values used in the code as well as calculations are as follows:

**Rotation speed** N: 4500 rpm  
**Geometry:** shaft diameter D 54.766 mm  
bearing diameter d 54.838 mm  
total length L 24.420 mm

**Lubricant:** absolute viscosity  $n_3(100^\circ \text{C}) = 3.40 \cdot 10^{-3} - 5.04 \cdot 10^{-3} - 7.42 \cdot 10^{-3} - 11.02 \cdot 10^{-3}$  Pa.s

**Macrotopography:**  $W_{AC} = 1.33 \mu\text{m}$   $\sigma = 1.32 \mu\text{m}$  ( $\sigma_{po}$ )  
 $W_{AL} = 1.04 \mu\text{m}$

**Surface texture profile A**  $W_{SmC} = 8000 \mu\text{m}$   
 $W_{SmL} = 1580 \mu\text{m}$

$W_{AC} = 1.90 \mu\text{m}$   $\sigma = 1.00 \mu\text{m}$   
 $W_{AL} = 0.34 \mu\text{m}$   
**Surface texture profile B**  $W_{SmC} = 8000 \mu\text{m}$   
 $W_{SmL} = 509 \mu\text{m}$   
 $W_{AC} = 2.80 \mu\text{m}$   $\sigma = 9.05 \mu\text{m}$   
 $W_{AL} = 10.0 \mu\text{m}$

**Surface texture profile C**  $W_{SmC} = 8000 \mu\text{m}$   
 $W_{SmL} = 646 \mu\text{m}$

**Microtopography:**  $\sigma_{poi}$  RMS (standard deviations) of the points altitudes measured distribution function,  $\sigma_{poi} = 0.00 \mu\text{m}$  (smooth bearing),  $\gamma_2 = 3.00$ ,  $\sigma_{po2} = 1.32 \mu\text{m}$ ,  $1.00 \mu\text{m}$  and  $9.05 \mu\text{m}$  for the cases A, B and C respectively.

**Load W** (in steady state conditions): 1500 - 3000 - 4500 N

Theoretical results are given in the following tables and figures.

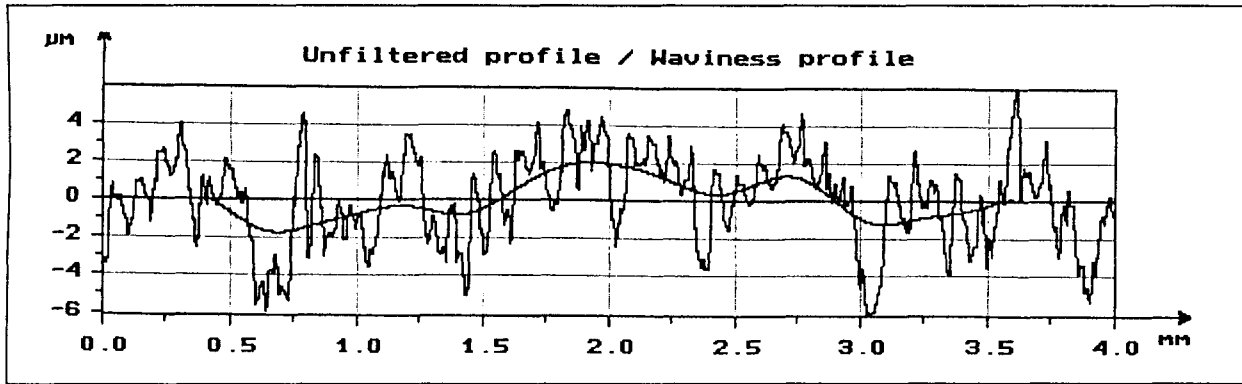


Fig. 2a Surface texture profile in lathe designation B (very low feed rate)  
 $s = 0.08 \text{ mm.rev}^{-1}$ ,  $v = 210 \text{ m.min}^{-1}$ ,  $R_a = 1.48 \mu\text{m}$ ,  $W_a = 0.92 \mu\text{m}$ ,  $R_{sm} = 102 \mu\text{m}$ ,  $W_{sm} = 1583 \mu\text{m}$

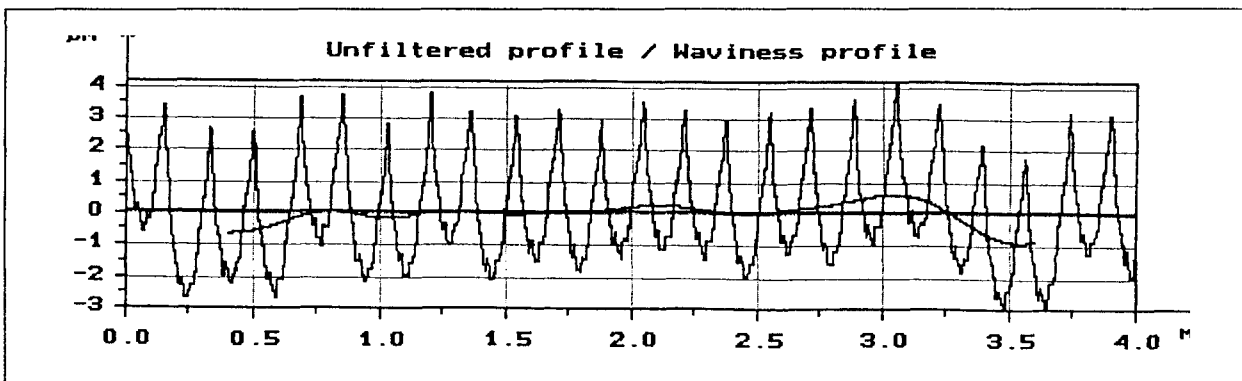


Fig. 2b Surface texture profile in lathe designation B (low feed rate for finishing)  
 $s = 0.16 \text{ mm.rev}^{-1}$ ,  $v = 210 \text{ m.min}^{-1}$ ,  $R_a = 1.20 \mu\text{m}$ ,  $W_a = 0.227 \mu\text{m}$ ,  $R_{sm} = 170 \mu\text{m}$ ,  $W_{sm} = 509 \mu\text{m}$

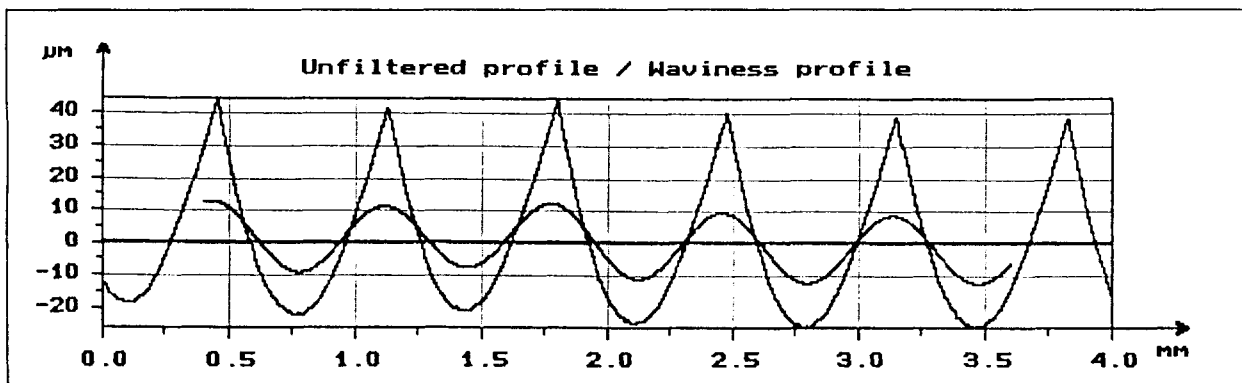


Fig. 2c Surface texture profile in lathe designation B (high feed rate)  
 $s = 0.60 \text{ mm.rev}^{-1}$ ,  $v = 210 \text{ m.min}^{-1}$ ,  $R_a = 10.8 \mu\text{m}$ ,  $W_a = 6.86 \mu\text{m}$ ,  $R_{sm} = 648 \mu\text{m}$ ,  $W_{sm} = 646 \mu\text{m}$

Table 7: Calculated results for smooth journal bearing surfaces,  $N=4500$  rpm Load  $W=1500$  N

Viscosity $n \cdot 10^{-3}$ [Pa.s]	Eccentricity $e$ [ $\mu\text{m}$ ]	Equil. angle $\alpha$ [ $^\circ$ ]	Mini film thick- ness $h$ [ $\mu\text{m}$ ]	Max. Pressure $10^6$ [Pa]	Shaft Friction Force [N]	Bearing Friction Force [N]
3.40	28.40	130.20	7.60	3.8	3.48	2.70
5.04	26.50	134.05	9.50	3.4	5.03	4.34
7.42	24.20	138.50	11.80	3.0	7.39	6.80
11.02	21.40	143.50	14.60	2.6	11.20	10.70

Table 8: Calculated results for smooth journal bearing surfaces,  $N=4500$  rpm. Load  $W=3000$  N

Viscosity $n \cdot 10^{-3}$ [Pa.s]	Eccentricity $e$ [ $\mu\text{m}$ ]	Equil. angle $\alpha$ [ $^\circ$ ]	Mini film thick- ness $h$ [ $\mu\text{m}$ ]	Max. Pressure $10^6$ [Pa]	Shaft Friction Force [N]	Bearing Friction Force [N]
3.40	31.20	123.8	4.80	9.5	4.00	1.97
5.04	29.70	127.4	6.30	8.3	5.37	3.64
7.42	27.99	131.2	8.00	7.4	7.53	6.00
11.02	26.00	135.1	10.00	6.6	10.97	9.65

Table 9: Calculated results for smooth journal bearing surfaces,  $N=4500$  rpm. Load  $W=4500$  N

Viscosity $n \cdot 10^{-3}$ [Pa.s]	Eccentricity $e$ [ $\mu\text{m}$ ]	Equil. angle $\alpha$ [ $^\circ$ ]	Mini film thick- ness $h$ [ $\mu\text{m}$ ]	Max. Pressure $10^6$ [Pa]	Shaft Friction Force [N]	Bearing Friction Force [N]
3.40	32.40	120.7	3.60	16.3	4.73	1.16
5.04	31.20	123.9	4.80	14.1	5.94	2.92
7.42	29.90	127.0	6.10	13.0	7.98	5.26
11.02	28.20	130.8	7.80	11.6	11.22	8.85

Table 10: Calculated results for surface texture profile A,  $N=4500$  rpm. Load  $W=1500$  N,

\* means roughness interaction ( $h < 3 \sigma$ )

Viscosity $n \cdot 10^{-3}$ [Pa.s]	Eccentricity $e$ [ $\mu\text{m}$ ]	Equil. angle $\alpha$ [ $^\circ$ ]	Mini film thick- ness $h$ [ $\mu\text{m}$ ]	Max. Pressure $10^6$ [Pa]	Shaft Friction Force [N]	Bearing Friction Force [N]
3.40**	29.2	131.6	5.53	3.4	3.54	2.55
3.40**	28.0	128.3	5.65	4.3	3.63	2.55
5.04	27.2	135.9	7.40	3.2	5.02	4.23
5.04	26.2	132.0	7.44	3.8	5.16	4.22
7.42	24.8	140.0	9.94	3.1	7.33	6.70
7.42	24.0	137.1	9.64	3.2	7.50	6.69
11.02	22.0	145.6	12.73	2.9	11.06	10.55
11.02	21.3	142.6	12.34	2.7	11.24	10.60

Table 11: Calculated results for surface texture profile A,  $N=4500$  rpm. Load  $W=3000$  N,

\* means roughness interaction ( $h < 3 \sigma$ )

Viscosity $n \cdot 10^{-3}$ [Pa.s]	Eccentricity $e$ [ $\mu\text{m}$ ]	Equil. angle $\alpha$ [ $^\circ$ ]	Mini film thick- ness $h$ [ $\mu\text{m}$ ]	Max. Pressure $10^6$ [Pa]	Shaft Friction Force [N]	Bearing Friction Force [N]
3.40	31.8	124.9	2.93*	7.6	4.38	1.54
3.40	30.6	121.7	3.00*	11.5	4.47	1.53
5.04	30.5	128.5	4.24	6.9	5.67	3.27
5.04	29.4	125.0	4.25	10.4	5.80	3.22
7.42	28.8	132.6	5.93	6.7	7.62	5.73
7.42	27.8	128.8	5.84	8.8	7.87	5.67
11.02	26.7	137.0	8.04	6.4	10.93	9.42
11.02	25.7	133.6	7.94	7.9	11.22	9.41

Table 11: Calculated results for surface texture profile A, N= 4500 rpm. Load W=3000 N,  
\* means roughness interaction ( $h < 3 \sigma$ )

Viscosity n.10 <sup>-3</sup> [Pa.s]	Eccentricity e [μm]	Equil. angle α [°]	Mini film thick- ness h [μm]	Max. Pressure 10 <sup>6</sup> [Pa]	Shaft Friction Force [N]	Bearing Friction Force [N]
3.40	31.8	124.9	2.93*	7.6	4.38	1.54
3.40	30.6	121.7	3.00*	11.5	4.47	1.53
5.04	30.5	128.5	4.24	6.9	5.67	3.27
5.04	29.4	125.0	4.25	10.4	5.80	3.22
7.42	28.8	132.6	5.93	6.7	7.62	5.73
7.42	27.8	128.8	5.84	8.8	7.87	5.67
11.02	26.7	137.0	8.04	6.4	10.93	9.42
11.02	25.7	133.6	7.94	7.9	11.22	9.41

Table 12: Calculated results for surface texture profile A, N= 4500 rpm. Load W=4500 N,  
\* means roughness interaction ( $h < 3 \sigma$ )

Viscosity n.10 <sup>-3</sup> [Pa.s]	Eccentricity e [μm]	Equil. angle α [°]	Mini film thick- ness h [μm]	Max. Pressure 10 <sup>6</sup> [Pa]	Shaft Friction Force [N]	Bearing Friction Force [N]
3.40	33.0	120.9	1.73*	15.1	5.79	0.10
3.40	31.8	118.5	1.84*	21.1	5.70	0.20
5.04	32.0	124.3	2.73*	12.5	6.70	2.04
5.04	30.7	121.6	2.94*	17.4	6.70	2.22
7.42	30.5	128.5	4.28	10.2	8.27	4.82
7.42	29.3	125.3	4.34	14.7	8.47	4.80
11.02	28.8	132.6	5.93	9.9	11.32	8.53
11.02	27.8	128.9	5.84	13.1	11.68	8.42

Table 13: Calculated results for surface texture profile B, N= 4500 rpm. Load W=1500 N,  
\* means roughness interaction ( $h < 3 \sigma$ )

Viscosity n.10 <sup>-3</sup> [Pa.s]	Eccentricity e [μm]	Equil. angle α [°]	Mini film thick- ness h [μm]	Max. Pressure 10 <sup>6</sup> [Pa]	Shaft Friction Force [N]	Bearing Friction Force [N]
3.40	29.5	132.4	5.84	3.5	3.56	2.51
3.40	27.8	127.5	5.94	4.7	3.71	2.50
5.04	27.5	136.9	7.84	3.5	5.02	4.20
5.04	26.0	131.8	7.77	4.1	5.22	4.18
7.42	25.2	141.4	10.14	3.4	7.31	6.66
7.42	23.8	136.7	9.97	3.5	7.56	6.68
11.02	22.1	146.8	13.24	3.2	11.04	10.56
11.02	21.2	142.1	12.57	2.9	11.30	10.58

Table 14: Calculated results for surface texture profile B,  $N=4500$  rpm. Load  $W=3000$  N,  
\* means roughness interaction ( $h < 3 \sigma$ )

Viscosity $n \cdot 10^{-3}$ [Pa.s]	Eccentricity $e$ [ $\mu\text{m}$ ]	Equil. angle $\alpha$ [ $^\circ$ ]	Mini film thick- ness $h$ [ $\mu\text{m}$ ]	Max. Pressure $10^6$ [Pa]	Shaft Friction Force [N]	Bearing Friction Force [N]
3.40	32.2	124.9	3.14	8.0	4.68	1.20
3.40	30.5	120.5	3.28	13.2	4.79	1.22
5.04	30.8	129.2	4.54	7.1	5.73	3.14
5.04	29.0	124.6	4.78	10.5	5.91	3.16
7.42	29.2	133.3	5.62	7.2	7.16	5.62
7.42	27.5	128.3	5.60	9.4	9.36	5.60
11.02	26.9	138.2	8.44	6.8	6.77	9.40
11.02	25.5	133.0	8.27	7.8	7.81	9.35

Table 15: Calculated results for surface texture profile B,  $N=4500$  rpm. Load  $W=4500$  N,  
\* means roughness interaction ( $h < 3 \sigma$ )

Viscosity $n \cdot 10^{-3}$ [Pa.s]	Eccentricity $e$ [ $\mu\text{m}$ ]	Equil. angle $\alpha$ [ $^\circ$ ]	Mini film thick- ness $h$ [ $\mu\text{m}$ ]	Max. Pressure $10^6$ [Pa]	Shaft Friction Force [N]	Bearing Friction Force [N]
3.40	33.2	121.7	2.40*	15.1	6.21	0.40
3.40	31.5	117.6	2.27*	22.2	6.15	0.20
5.04	32.2	124.9	3.14	11.9	6.94	1.78
5.04	30.5	120.5	3.27	19.6	7.10	1.81
7.42	30.8	129.2	4.54	10.4	8.44	4.62
7.42	29.2	124.1	4.58	16.6	8.84	4.48
11.02	29.2	133.3	6.14	10.6	11.42	8.34
11.02	27.5	128.4	6.27	13.9	11.87	8.32

Table 16: Calculated results for surface texture profile C,  $N=4500$  rpm. Load  $W=1500$  N,  
\* means roughness interaction ( $h < 3 \sigma$ )

Viscosity $n \cdot 10^{-3}$ [Pa.s]	Eccentricity $e$ [ $\mu\text{m}$ ]	Equil. angle $\alpha$ [ $^\circ$ ]	Mini film thick- ness $h$ [ $\mu\text{m}$ ]	Max. Pressure $10^6$ [Pa]	Shaft Friction Force [N]	Bearing Friction Force [N]
3.40			Contacts			
3.40			Contacts			
5.04			Contacts			
5.04			Contacts			
7.42			Contacts			
7.42			Contacts			
11.02	20.5	149.6	5.03*	3.45	11.21	10.78
11.02	19.42	136.4	3.82*	10.00	12.24	10.30

Table 17: Calculated results for surface texture profile C,  $N = 4500$  rpm. Load  $W = 3000$  N,  
\* means roughness interaction ( $h < 3 \sigma$ )

Viscosity $n \cdot 10^{-3}$ [Pa.s]	Eccentricity $e$ [ $\mu\text{m}$ ]	Equil. angle $\alpha$ [ $^\circ$ ]	Mini film thick- ness $h$ [ $\mu\text{m}$ ]	Max. Pressure $10^6$ [Pa]	Shaft Friction Force [N]	Bearing Friction Force [N]
3.40			Contacts		,	
3.40			Contacts		,	
5.04			Contacts		,	
5.04			Contacts		,	
7.42			Contacts		,	
7.42			Contacts		,	
11.02	25.5	141.0	0.50*	14.0	11.54	9.03
11.02	22.6	123.8	0.60*	93.6	16.57	5.03

Table 18: Calculated results for surface texture profile C,  $N = 4500$  rpm. Load  $W = 4500$  N,  
\* means roughness interaction ( $h < 3 \sigma$ )

Viscosity $n \cdot 10^{-3}$ [Pa.s]	Eccentricity $e$ [ $\mu\text{m}$ ]	Equil. angle $\alpha$ [ $^\circ$ ]	Mini film thick- ness $h$ [ $\mu\text{m}$ ]	Max. Pressure $10^6$ [Pa]	Shaft Friction Force [N]	Bearing Friction Force [N]
3.40			Contacts		,	
3.40			Contacts		,	
5.04			Contacts		,	
5.04			Contacts		,	
7.42			Contacts		,	
7.42			Contacts		,	
11.02	28.4	138.6	Contacts	40.2	11.70	8.10
11.02	26.2	126.6	Contacts	60.2	13.24	7.40

\*\* The first row represents theoretical results for a given waviness configuration and the second one for the same waviness configuration rotated by 90 degrees clockwise.

## 5. CONCLUSIONS

The following conclusions may be drawn from the presented experimental-analytical study:

- ▶ Excellent or very good correlation is established between roughness CLA value  $R_a$  and relevant waviness parameters, which enabled the formulation of exponential regression models. The essence of this fact is that waviness appears to be affected in some extent by cutting factors.
- ▶ Circumferential waviness is greater than axial waviness and greater again than circumferential roughness.
- ▶ Waviness is of harmonic form in the range of high feed rates, whereas it appears to obtain random shape at low and medium feed rates.
- ▶ Simulated results of journal bearing tribological behaviour show that the lubrication regime is not fully hydrodynamic. The minimum film thickness for the obtained results is not higher than  $1.3 \mu\text{m}$  but hydrodynamic shaft - bearing friction losses are very low. This is finding consistent with results found by various authors ( $\mu < 0.05$ ). More experimental research work in the area of shaft - bearing friction losses would eventually confirm various parameter influences by comparing computed and experimental results.

- ▶ In the lubrication analysis of finite bearing, the effect of both longitudinal and circumferential roughness and waviness has been considered significant. This effect is a three-dimensional variation of oil film thickness and pressure and it is studied by an average Reynolds equation through an algorithmic scheme in order to calculate contact geometry and friction between shaft and bearing under dynamic load.
- ▶ From the cases under study, low feed rates provide the best results offering perspective for the establishment of turning operations in finishing of shafts. Very low feed rates result in increase of axial roughness and waviness, which destroy hydrodynamic load support mechanism, even with the generated higher circumferential waviness value. This effect appears to be more significant for low speed, low viscosity and high load.

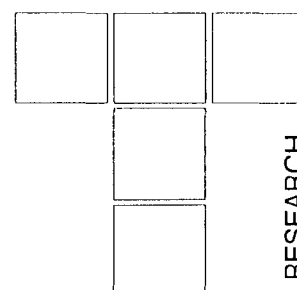
The present work creates a basis for a new improved analysis of the problem concerning bearing behaviour and its system performance in detail when a combination of roughness and waviness is considered for the lubricated surfaces. In the authors' opinion, there must be carried out an exhaustive investigation too into the particular shaft-bearing surface texture characteristics every individual machining process creates, taking into account the evaluation and analysis of roughness-waviness combination regarded from the tribological standpoint.

## REFERENCES

- [1] Arnold O., Schultheiss H. and Glaser H., "Experimental investigation into the oil flow rate and the friction moment of dynamically loaded plain journal bearings", Proceedings INTERTRIBO '99, Slovak Republic, 1999.
- [2] Cameron A., "Basic Lubrication theory", Ellis Horwood Ltd, 1981.
- [3] Christensen H., "Stochastic Models for Hydrodynamic Lubrication of Rough Surfaces", Proc. Inst. Mech. Eng. Tribology Group 184, Part 1, Vol. 55, 1970.
- [4] Christensen H., "A Theory of Mixed Lubrication", Proc. Inst. Mech. Eng., Vol. 186, 1972.
- [5] Dagnall M.A., "Exploring surface texture", Rank Taylor Hobson Ltd, Leicester, 2nd edition, 1986.
- [6] Dimofte F., "Bearings with non-conventional geometry (or wave bearings)-an advanced bearing technology", Proc. 3rd Int. Conf. BALKANTRIB '99, 1999.
- [7] Greenwood J.A., "The area of contact between rough surfaces and flats", Journal of Lubrication Technology, January 1967.
- [8] Greenwood J.A. and Tripp J.H., "The contact of two nominally flat rough surfaces", Proc. Inst. of Mech. Eng., Vol. 185, 1971.
- [9] Handzel-Powierza Z., Klimczak T. and Polijaniuk A., "On the experimental verification of the Greenwood-Williamson model for the contact of rough surfaces", Wear 154 (1992) 115-124.
- [10] Kruszynski B. and van Luttervelt K.A., "The influence of manufacturing processes on surface properties", Adv.Manuf.Engg 1, 1989, pp.187-202.
- [11] Lin J.R., "Steady state performance of finite Hydrodynamic journal bearing with three-dimensional irregularities", ASME, J. Tribol. 112 (1990) 497-505.
- [12] Lin J.R., "Squeeze film characteristics of finite journal bearings: couple stress fluid model", Tribology Intern. Vol. 31, Nr 4 (1998) 201-207.
- [13] Noizat J., "Viscosite limite admissible des lubrifiants faible viscosite dans les paliers", E.C.L-DLA/DRDA/RNUR, Paris 1985.
- [14] Pandazaras C.N., "Etudes Experimentales et Theoriques sur les Pertes par Frottement dans les Ensembles Pistons-Segments-Chemises", Etude Bibliographique, DLA/DRDA/RNUR - ISMCM, France, 1982.
- [15] Pandazaras C.N., "Modelisation du Frottement Segment-Chemise", DLA/DRDA/RNUR, Note Technique No 5781, France, 1982.
- [16] Pandazaras C.N., "Influence de la Forme des Segments sur le Frottement Segment-Chemise", DLA/DRDA/RNUR, Note Technique No 5808, France, 1983.
- [17] Pandazaras C.N., "Modelisation Theorique et Experimentale du Frottement Segment-Chemise", These D.D.I., ISMCM-DLA/DRDA/RNUR, France, 1985.
- [18] Pandazaras C.N., "RENAULT Ring-Liner Friction Code", JRC-PG Tribology in Power Train, (PSA-FIAT-VOLVO-B.L.-RENAULT) DLA/DRDA/RNUR, France, 1985.
- [19] Pandazaras C., Petropoulos G and Koutlas G., "Numerical Modelling of the Functional Behaviour of Finite Sliding Hydrodynamically Lubricated Journal Bearings Considering Surface Macrogeometrical Deviations and Dynamic Loading", Journal of the Balkan Tribological Association, Vol.5, No 3, 1999.
- [20] Patir N. and Cheng H.S., "An average model for determining effects of three dimensional roughness on partial hydrodynamic lubrication", Trans. ASME, vol. 100, 1978.
- [21] Patir N. and Cheng H.S., "Application of average flow model to lubrication between rough sliding surfaces", Trans. ASME, vol 101, 1979.
- [22] Peters J. and al, "Assessment of surface typology analysis techniques", Annals of the CIRP, 28/2, 1979, pp. 539-553.
- [23] Petropoulos P., "A note on the homogeneity of the roughness on oblique finish turned surfaces", Wear, 24,1973, pp.147-152.
- [24] Petropoulos G., Pandazaras C. and Stamos I., "Developing predictive models between selected texture parameters of turned surfaces", Journal of Balkan Tribological Association, Vol.5, No 3, 1999.
- [25] Pranab K.Das, "Analysis of Piston Ring Lubrication", SAE Paper 760008, 1976.
- [26] Rank Taylor Hobson, Handbook, Version 1.1.1, 1995.
- [27] Rasheed H.E., "Effect of surface waviness on the hydrodynamic Lubrication of plain cylindrical sliding element bearing", WEAR 223 (1998) 1-6.
- [28] Rohde S.M., "A mixed friction model for dynamically loaded contacts with application to piston ring lubrication", General Motors Research Laboratories, 1980.
- [29] Strzelecki S. and Someya T., "Static characteristics of the off-set halves journal bearing", Proceedings INTERTRIBO '99, Slovak Republic, 1999.
- [30] Strzelecki S., "Journal centre trajectory of dynamically loaded offset-halves bearing", Proceedings BALKANTRIB '99, Sinaia-Romania 1999.
- [31] Strzelecki S., "Friction Loss of 2-lobe journal bearing with different bush profile", Proceedings BALKANTRIB '99, Sinaia-Romania 1999.
- [32] Teale J.L. and Lebeck A.O., "An evaluation of the Average flow model for surface roughness effects in lubrication", Trans. ASME, vol 102, 1980.
- [33] Tripp, J.H., "Surface roughness effects in hydrodynamic lubrication: the flow factor method", Transactions of the ASME, Vol. 105, 1983.
- [34] Tzeng, S.T. and Saibel, E., "Surface roughness effects on slider bearing lubrication" ASLE, Vol. 10, 1967, p.334.
- [35] Whitehouse D.J., "Handbook of surface metrology", Institute of Physics publishing for Rank Taylor Hobson Co, Bristol, 1996.
- [36] Zhang G.M. and Kapoor S.G., "Dynamic generation of machined surfaces, Part 2, Construction of surface topography", Journal of Engineering for Industry, Vol. 113, May 1991.

M. KUZINOVSKI, P. CICHOSZ, H. ZEBROWSKI, Z. STAMBOLISKA

# Research of The Correlation Between The Two-dimensional and Three-dimensional Roughness of The Machined Surfaces at Increased Speed of Turning



Presented results and seeings represent a part of the researches activities realized within the International project whose main goal is development of methods for researching and creation of technological surface layer with in advance known and repeatable characteristics. These researches are referring to turned surfaces machined with increased speeds of cutting. The machined material is C 1630 (DIN C 55). Turning was performed on NC lathe TUR 50 SN-DC with power  $P=18,5kW$  and ceramic cutting plates MC2 from the firm HERTEL. A four-factor plan of experiments is applied. The turning was performed under the machined terms of:  $v=300-500$  (m/min),  $f=0,16-0,32$  (mm/2  $\pi$  rad),  $a=0,5-1,6$  (mm) and  $r=1,2-2,0$  (mm). The measurements of the 2-D and 3-D roughness parameters of the height surface distribution are carried out with the computerized device FORM TALYSURF-120L from the firm Taylor Hobson (Wroclaw Polytechnic). A comparative analysis and correlation between the height distribution 2-D and 3-D roughness parameters of turned surface are given.

**Keywords:** correlation, two-dimensional, three-dimensional, roughness, parameters

## 1. INTRODUCTION

Surface layer of the machined surfaces is the basic factor in the realization of different functions of the mechanical parts. Physico-chemical characteristics of the zones of the technological surface layer (TSL) and the geometric structure (GS) of the TSL surface take active role in the performance of the numerous static processes (contact realization, stiffness, conductivity, reflexivity, etc) and dynamical processes (tribological processes, lubrication etc) [1] during parts exploitation. Roughness of the machined surfaces (MS), which represents the micro GS of the TSL surface, influence the constitution of the MS exploitation properties [2] through the characteristics of the surface high distribution, shape, curvature and slope of the irregularities and texture directionality. Two main admissions [3], are in use for description of the roughness characteristics and roughness influence on the exploitation properties. One of them is defined in two-dimensional, while other is defined in three-dimensional domain. The both admissions possess its ones advantages and faults, which define their applicability at different purposes.

M. Kuzinovski, Faculty of Mechanical Engineering, The "Sv.Kiril i Metodij" University, Skopje, Macedonia,  
P. Cichosz, H. Zebrowski, Institute of Mechanical Engineering and Automation of the Technical University of Wroclaw, Wroclaw, Poland  
Z. Stamboliska, Skopje, Macedonia

## 2. COMPARATIVE ANALYSIS OF THE TWO-DIMENSIONAL AND THREE-DIMENSIONAL CHARACTERIZATION OF THE ROUGHNESS

The analysis of the state in the area of roughness characteristic research, carried out within the International project, shows the presence of the two main groups of activities [3]:

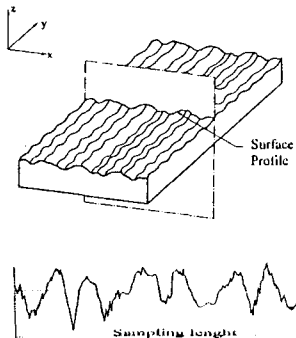
- defining of the dependency between the characteristics of the formed surface topography on the MS and the mechanism of its generation, and
- determination of the correlation between the formed TSL and its functional behavior under exploitation terms.

Design of an embraced experimental and analytical base that will unite the both groups of activities, will enable constitution of a TSL that possess geometrical and physico-mechanical characteristics which can provide the in advance known and needed exploitation properties of the TSL. Solution of this problem can be achieved only by the application of the adequate technique for characterization [4] of the surface topography, which includes visual and numerical techniques for description and interactive methods for modeling the surface topography.

However, it is obvious that certain polemics is present among the science researchers in relation to the 2-D characterization and 3-D characterization of the GS of the TSL surface. The attitude still exists that 3-D characterization should longer stay as a tool used only for laboratory investigations. Such a state can be explained with the fact that 2-D characterization is much simpler in comparison to the 3-D characterization.

From the other side, it has been found that 2-D characterization is still not completely accepted and explained, especially from the point of determination the influence that generated 2-D roughness parameters have on the functional characteristics of the mechanical parts under exploitation. Also, it has been ascertained that application of the 2-D characterization for prediction of the MS functional behavior is basically wrong from many reasons, but the essential reason is the fact that all contacts between the mutually active MS have three-dimensional nature.

Table 1. Classification of 2-D roughness parametes

2-D ROUGHNESS PARAMETERS	
<p><b>AMPLITUDE PARAMETERS</b>  <math>R_p</math> - Max. profile peak height  <math>R_v</math> - Max. profile valley depth  <math>R_z</math> - Max. height of profile  <math>R_c</math> - Mean height of profile elements  <math>R_t</math> - Total height of profile  <math>R_a</math> - Arithmetical mean deviation of the assessed profile  <math>R_q</math> - Root mean square deviation of the assessed profile  <math>R_{sk}</math> Skeweness of the assessed profile  <math>R_{ku}</math> - Kurtosis of the assessed profile</p>	<p><b>CURVES AND RELATED PARAMETERS (FUNCTIONAL PARAMETERS)</b>  <math>Ml\textcircled{C}</math> - Profile bearing length  <math>Rmr\textcircled{C}</math> - Material ratio of the profile  <math>R\delta c</math> - Profile section height difference  <math>Rmr</math> - Relative material ratio</p>
<p><b>SPACING PARAMETERS</b>  <math>RSm</math> - mean width of the profile elements  <math>S</math> - mean spacing of local peaks of the profile  <math>L_o</math> - developed profile length  <math>l_r</math> - profile length ratio  <math>D</math> - profile peak density</p>	<p><b>FUNCTIONS OF THE ROUGHNESS PROFILE</b>  <math>ACF</math> - Profile autocorrelation function  <math>GSM</math> - Spectral power density of the profile  <math>VFG</math> - Probability density function of the profile</p>
<p><b>HYBRID PARAMETERS</b>  <math>\bar{\theta}</math> - Profile slope angle  <math>R_{\Delta a}</math> - Arithmetical mean slope of the profile  <math>R_{\Delta q}</math> - Root mean square slope of the assessed profile  <math>\lambda_a</math> - Average wavelength of the profile  <math>\lambda_q</math> - Root-mean-square wavelength of the profile</p>	

2-D characterization of the MS roughness creates presentation of its characteristics under the basis of the data logged from the roughness profile. This profile is obtaining with the section of a vertical plane and measured surface. But this section may not cross the real peaks and valleys. Because of that, all the values of the parameters that are determined from the roughness profile within the several sampling lengths (Table 1, Fig. 1) [3, 5, 6] may represent only approximation of the real values [3, 4]. In this way, their physical meaning did not allow correct determination of the surface behavior under different exploitation terms.

3-D characterization of the roughness is performed under the basis of the data logged from the real three-dimensional surface. During the logging of this kind of datapoints, measurement processes enable obtaining of the real peaks and valleys. At the same time, these data are more numerous what provides them better independence [4]. The improvement of the measurement instruments [1, 7] on a level that enable logging of three-

dimensional data from the surface gave the opportunity for development of 3-D roughness parameters.

A part of this system of parameters is directly obtained from the 2-D parameters that have utilitied meaning, while other are specially developed for description of the three-dimensional characteristics of the micro GS and for the functional characteristics of the MS. They are determined within a sampling area (Table 2, Fig.2) [4, 6, 7]. Taking into account all these facts, 3-D characterization enables more realistic presentation of the natural properties of the surface topography: the size, the shape and the volumes of the three-dimensional features [4, 9].

Differences, which appear between the 2-D and 3-D characterization, are specially prominent in determination of the bearing area curve. The bearing curve that is obtained from the 3-D datapoints is more realistic in comparison to the bearing curve obtained from the

roughness profile at 2-D characterization, what actually has no meaning of the real "area of bearing"[4]. This kind and many other differences which appear between the certain parameters values, are specially significant at the stochastic surfaces generated with the machining processes of grinding, sand blasting, electro-discharge etc [4].

The properties of the 3-D roughness characterization to create quantitative and qualitative [4, 9] presentation of the real state of the surface topography give possibility for all macro and micro influences, which are present in the constitution of the TSL, to be surveyed and which at the same time can be neglected in the 2-D characterization.

Additional advantage of the 3-D characterization is the possibility to provide new information important for the engineers and tribologists which give information for the prediction of the surface functionality. They are provided through the visualization of the surface topography

Table 2. Classification of 3-D roughness parametes

3-D ROUGHNESS PARAMETERS	
<b>AMPLITUDE AND HEIGHT DISTRIBUTION PARAMETERS</b> $S_a$ - Arithmetical mean deviation $S_z$ - Ten point height of the surface $S_q$ - Root-mean-square deviation $S_{sk}$ - Skeweness of surface height distribution $S_{ku}$ - Kurtosis of surface height distribution	<b>FUNCTIONAL PARAMETERS</b> $S_{bi}$ - Surface bearing index $S_{ci}$ - Core fluid retention index $S_{vi}$ - Valley fluid retention index
<b>SPATIAL PARAMETERS</b> $S_{ds}$ - Density of summits of the Surface $S_{tr}$ - Texture aspect ratio of the Surface $S_{td}$ - Texture direction of the surface $S_{al}$ - Fastest decay autocorrelation lenght	<b>FUNCTIONS OF THE SURFACE ROUGHNESS</b> $AACF$ - Areal autocorrelation function
<b>HYBRID PARAMETERS</b> $S_{sc}$ - Arithmetic mean summit curvature of the surface $S_{\Delta q}$ - Root-mean-square slope of the surface $S_{dr}$ - Developed interfacial area ratio	

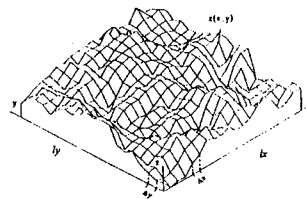


Figure 2: Sampling area [4]

[3, 4] and determination of the size of the contact area, debris volume, volume of the lubricant oil [3] etc. Namely, a modification of the parameters meaning and their mathematical interpretation is noticed. This modification is going in a direction that will provide better functional, direct or in-direct characterization of the machined surfaces [3, 11].

### 3. CORRELATION BETWEEN THE TWO-DIMENSIONAL AND THREE-DIMENSIONAL ROUGHNESS OF THE MACHINED SURFACES EXPRESSED THROUGH AN EXAMPLE OF A TURNED SURFACE

The correlation between the 2-D and 3-D characterization of the MS is analyzed on an example of a turned surface. The influences of the technological parameters on the modification of the roughness characteristics are determined with the aim to define the dependency between the characteristics of the formed surface topography and the mechanism for its constitution [3, 5].

Developed mathematical models describe the nature of the accomplishment of the influence that technological parameter has on the TSL constitution.

Parallel measurements of 2-D roughness profile measurement and 3-D measurement of an area from the same turned surface were performed. The measurement surface was obtained with turning using the cutting inserts SNGN 120712-120716-120720 from metallo-ceramic MC2 (Al<sub>2</sub>O<sub>3</sub> + TiC) (HERTEL), placed into the toolholder CSRNR 25x25 M12N3 (HERTEL), which gives the following stereometry to the cutting tool:

$$\begin{aligned} \kappa &= 75^\circ, \kappa_1 = 15^\circ, \gamma = -6^\circ, \alpha = 6^\circ, \lambda = -6^\circ, \\ \varepsilon_r &= 90^\circ, \gamma_f = 20^\circ, b_f = 0.2 \text{ mm} \end{aligned}$$

A carbon steel S1630 (DIN C55) with hardness within: 200 to 217 HB was adopted as a work material. Numerically controlled lathe TUR 50 SN-DG with power of 18.5 kW and interval of steepless change of the revolutions  $n=50-2250 \text{ o/min}$  was used. Measurement of the roughness parameters was performed using computerized measurement device FORM TALYSURF 120L[2], following the recommendation from [5, 8].

Turning was performed without use of the coolant, changing the cutting speed  $v$ , feed  $f$ , depth of cut  $a$  and the corner radius  $r_e$  (Table 3).

Obtained experimental values of the 2-D and 3-D roughness parameters are presented in Table 3.

Table 3. Parameters of 2-D roughness and 3-D roughness obtained from the measured turned surface

EXPERIMENT DESIGN MATRIX					SUBORDINATED VARIABLES									
Br.	$v_c$ m/min	$f$ mm/o	$a_p$ mm	$r_e$ mm	Ra $\mu\text{m}$	Rv $\mu\text{m}$	Rp $\mu\text{m}$	Rt $\mu\text{m}$	Rq $\mu\text{m}$	sRa $\mu\text{m}$	sRv $\mu\text{m}$	sRp $\mu\text{m}$	sRt $\mu\text{m}$	sRq $\mu\text{m}$
1	300	0.16	0.5	1.2	0.939	2.42	2.850	5.260	1.129	0.675	2.22	2.21	4.43	0.819
2	500	0.16	0.5	1.2	0.700	2.46	2.400	4.900	0.889	0.623	1.32	1.88	3.2	0.73
3	300	0.32	0.5	1.2	2.696	4.166	7.633	11.80	3.180	1.77	3.52	5.87	9.39	2.157
4	500	0.32	0.5	1.2	2.32	4.166	6.960	11.15	2.750	1.909	2.5	5.63	8.13	2.251
5	300	0.16	1.6	1.2	0.763	2.200	2.633	4.900	0.963	0.756	1.54	2.27	3.81	0.889
6	500	0.16	1.6	1.2	0.773	2.236	2.727	4.970	0.960	0.719	1.65	2.3	3.95	0.87
7	300	0.32	1.6	1.2	3.233	5.310	9.588	14.90	3.824	2.683	3.57	8.09	11.66	3.17
8	500	0.32	1.6	1.2	2.940	5.733	9.116	14.80	3.526	2.335	3.06	7.72	10.78	2.86
9	300	0.16	0.5	2.0	0.836	2.566	2.733	5.330	1.026	0.584	1.29	1.8	3.09	0.700
10	500	0.16	0.5	2.0	0.685	1.900	2.080	3.980	0.828	0.526	1.28	1.38	2.66	0.617
11	300	0.32	0.5	2.0	1.833	3.600	5.133	8.733	2.163	1.274	2.01	3.8	5.81	1.506
12	500	0.32	0.5	2.0	1.710	3.930	4.866	8.866	2.023	1.183	1.8	3.67	5.47	1.404
13	300	0.16	1.6	2.0	0.710	2.033	2.400	4.433	0.873	0.496	1.25	1.72	2.97	0.597
14	500	0.16	1.6	2.0	0.697	2.361	2.100	4.454	0.863	0.383	1.08	1.26	2.34	0.462
15	300	0.32	1.6	2.0	1.902	3.933	5.613	9.533	2.271	1.318	1.92	3.9	5.82	1.531
16	500	0.32	1.6	2.0	2.058	4.616	6.033	10.65	2.426	1.436	2.55	3.95	6.5	1.693
17	387	0.226	0.894	1.549	1.143	2.533	3.566	6.066	1.386	0.919	1.75	2.94	4.69	1.101
18	387	0.226	0.894	1.549	1.435	3.475	4.000	7.500	1.690	1.111	2.16	2.94	5.1	1.271
19	387	0.226	0.894	1.549	1.284	3.025	4.200	7.175	1.625	0.98	1.95	2.88	4.90	1.05
20	387	0.226	0.894	1.549	1.357	2.860	3.940	6.760	1.540	0.95	2.05	3.20	5.25	1.20

\* Sampling area 1.28 x 1.28, cut-off 0.425x0.425, Gaussian filter

Table 4. Overview of the mathematical models of the 2-D and 3-D roughness parameters

OVERVIEW OF THE MATHEMATICAL MODELS		
Without the mutual influence and the grade of the factor's significance	$Ra = 49.802 \cdot v^{-0.179} \cdot f^{1.587} \cdot a^{0.0415} \cdot r_E^{-0.463}$	$sRa = 30.139 \cdot v^{-0.133} \cdot f^{1.518} \cdot a^{0.066} \cdot r_E^{-0.824}$
	$Rq = 50.742 \cdot v^{-0.164} \cdot f^{1.534} \cdot a^{0.0468} \cdot r_E^{-0.472}$	$sRq = 35.921 \cdot v^{-0.1343} \cdot f^{1.512} \cdot a^{0.068} \cdot r_E^{-0.842}$
	$Rt = 80.312 \cdot v^{-0.069} \cdot f^{1.220} \cdot a^{0.0708} \cdot r_E^{-0.419}$	$sRt = 156.115 \cdot v^{-0.207} \cdot f^{1.236} \cdot a^{0.061} \cdot r_E^{-0.83}$
	$Rv = 10.581 \cdot v^{-0.0505} \cdot f^{0.954} \cdot a^{0.065} \cdot r_E^{-0.231}$	$sRv = 34.971 \cdot v^{-0.227} \cdot f^{0.835} \cdot a^{0.0187} \cdot r_E^{-0.709}$
	$Rp = 114.795 \cdot v^{-0.163} \cdot f^{1.431} \cdot a^{0.0785} \cdot r_E^{-0.549}$	$sRp = 139.023 \cdot v^{-0.204} \cdot f^{1.486} \cdot a^{0.0889} \cdot r_E^{-0.894}$

The analysis of the mathematical models (Table 4) of the appropriate height distribution parameters, determined in 2-D and 3-D domain, show the dominance of the MS roughness characteristics by the machining conditions [10].

The very strong influences of the feed and cutting speed are confirmed in the 2-D domain as in the 3-D domain. But, the mathematical models estimated on the basis of the 3-D measurement distinguish the small influences which can be neglected from the 2-D measurement. In certain cases, during the positioning of the 2-D measurement traces, certain errors can be recorded, which can cause appearance of a virtual difference in the influences that parameters show in the mathematical models. Greater distinction appears in relation to the influence of the **corner radius**  $r_E$ . 3-D measurements point at greater influence of its value on the height distribution characteristics of the micro GS. Such a constellation is confirmed by the fact that the corner of the cutting insert, depending on the cutting tool stereometry acts from a position, which does not match the position of the plane where 2-D roughness profile is measured. During the machining processes, the tool corner interferes with the material from the MS in three-dimensional space. This kind of acting distinguishes it from the **feed**, whose influence mainly reflexes in two-dimensional space, or more correct, in direction of the cutting edge movement. Because of this, much smaller differences appear in relation to the level of the feed influence.

**Depth of cut** has indirect influence on the modification of the roughness characteristics because it changes the conditions of the TSL constitution [5, 10]. Its enlargement causes very small increase of the height distribution characteristics where the greatest difference appears in relation to the maximal depth of valleys, as in the case of the cutting speed. The reasons for this may be result of the measurement nature where 3-D measurements take into account the three-dimensional acting of the cutting tip tool.

In relation to the cutting speed, the phenomenon of the multifarious influence on the roughness parameters appears. Results from 2-D domain show very soft increase of the valleys and decrease of all other parameters with

the enlargement of the cutting speed. At the same time 3-D measurement show uniform influence of the cutting speed on all parameters: they all decrease with the speed enlargement. Taking into account that cutting speed's influence is accomplished through the changes in the physics of the cutting process [5, 10], appearances of intensive vibrations can be expected when the speed increase above the certain level. This kind of vibrations causes modification of the process of chip dismounting from the basic material. This can result in eventual deepening of the valleys. But, the appearance of the vibrations would give as a result total deepening of the valleys in 3-D domain also, but that does not appear in this case.

One of the possible reasons, taking into account the very small positive influence in the equation for the  $Rv$  parameter, can be the selection of the measurement traces. The measurement trace can be placed in a position where some changes in the cutting process appeared only in the certain moment, but they were recorded as a representative for the whole surface. But in the reality, after these changes, a stabilization of the cutting process set in. So, with the three-dimensional measurement, datapoints are logged from large number parallel-positioned traces and they embrace a whole area from the same surface. This means that more correct conclusion can be drawn for the influence of this technological parameter on the constitution of the MS irregularities from this way measured datapoints.

#### 4. CONCLUSION

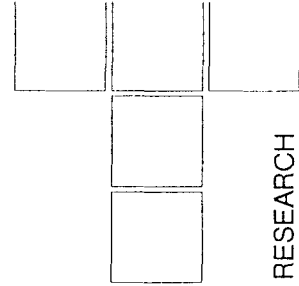
Presented mathematical models of the 2-D and 3-D roughness parameters confirm the analogy that exists in the both approaches to description of the influence that technological parameters have on the roughness characteristics on macro level. But, at the same time they point to the certain differences that order gradual shifting to 3-D roughness characterization and where 2-D characterization will certain period still be used as an initial basis for roughness analysis [3, 4]. The last constellation is above all governed by the fact that 3-D characterization of the roughness decreases the total measurement errors and in that way it contributes for the smaller

influences of the machining conditions in the process of TSL constitution to come to expression.

In our case of description of the height distribution characteristics, the advantages of 3-D characterization does not have that marked significance in relation to the errors that can appear in their values. But the application of 3-D roughness characterization, as a descriptor of the real state of the TSL micro GS, is the only mean that can provide correct determination of the functional parameters.

## REFERENCES

- [1.] *M. Kuzinovski, Z. Stamboliska*, Characteristics of three-dimensional geometric structure of the machined surfaces, International Conference on Advanced Mechanical Engineering & Technology AMTECH'99, Plovdiv, Bulgaria, 1999
- [2.] *Z. Stamboliska, M. Kuzinovski*: Research of the correlation between the parameters that describe the microstereometry and the exploitation properties of the technological surface layer, Conference SURFACE LAYER'99, Lubniewice, Poland, 1999 (to be printed)
- [3.] *M. Kuzinovski, V. Pavlovski, H. Zebrowski, P. Cichosz, Z. Stamboliska, J. Szymkowski, V. Gecevska*, Temporary methods for researching the 3-D geometric structure characteristics of the machined surfaces, science-research project financed by the Ministry of science of R. Macedonia, No. 40068498, 1998-2000
- [4.] *K. J. Stout*, Three-Dimensional Surface Topography; Measurement, Interpretation and Applications, A Survey and Bibliography, University of Birmingham, 1994
- [5.] *M. Kuzinovski*, Istrazuvanje na fizickite pojavi i tehnoloskite efekti pri struzenje so zgolemeni brzini na rezenje, Doctorate, Skopje, Macedonia, 1991
- [6.] ISO 4287, Geometrical Product Specifications- Surface texture: Profile method-Terms, definitions and surface texture parameters, 1997
- [7.] *M. Kuzinovski, Z. Stamboliska, P. Cichosz*, An overview of the state of the reseaches machined surfaces microstereometry areas, Sympozjum INZYNIERA POWIERZCHNI'99, Wroclaw, Poland, 1999
- [8.] *M. Kuzinovski, Z. Stamboliska, P. Cichosz*, Influence of the microstereometry measurement conditions on the accuracy of the obtained results, Sympozjum INZYNIERA POWIERZCHNI '99, Wroclaw, Poland, 1999
- [9.] *Z. Stamboliska, M. Kuzinovski*: Analysis and mathematical interpretation of parameters that describe the microstereometry of machined surfaces, BALKANTRIB'99, Sinaia, Romania, 1999
- [10.] *M. Kuzinnovski, S. Trajkovski, Z. Stamboliska*, Researches of the parameters that describe 3-D waviness and roughness of the turned surfaces machined with increased speed of cutting, HEAVY MACHINERY HM'99, Kraljevo, 1999 (in press)
- [11.] *Z. Stamboliska, M. Kuzinovski, P. Cichosz, J. Szymkowski*, Application of the skewness and kurtosis for identification of the characteristics of the machined surface geometric structure, Sympozjum INZYNIERA POWIERZCHNI'99 Wroclaw, Poland, 1999



C. GHEORGHIES, M. SIMIONOV

# Study on Tribomodel of The Damage Process in The Diesel Engine Cylinder Liners

*In order to study the developed structural changes in the surface layer of the cast-iron, used in manufacturing the Diesel engines cylinder liner, the tribosystem and tribomodel concepts are applied. Using the X-ray diffraction and microscopy methods, the evolutions and the distribution of the dislocations density, the internal second order tensions, as well as the microstructure modifications during fatigue and cavitation processes are displayed. These evolutions depend on the thickness of the tested samples and allow to establish the damage mechanisms of superficial layer during fatigue and cavitation process.*

**Keywords:** engine, cavitation, tribomodel, structure

## 1. INTRODUCTION

The tension state in the surface layer has an important influence upon the behaviour at the cavitation wear of the materials, generally, and on the Diesel engines cylinder liners from, specially [1, 9]. The carried out experimental researches are based on the tribomodel and tribosystem concepts that were defined in some papers [2, 3, 8]. A tribosystem was defined using the relative movement of the triboelements in contact, the type of the interposed element (lubricant, abrasive material) and the working medium. Four tribosystem types were defined: the sliding and sliding with rolling tribosystem, "T<sub>A</sub>", the rolling and rolling with sliding tribosystem, "T<sub>R</sub>", the abrasive tribosystem, "T<sub>Z</sub>", and the cavitation tribosystem, "T<sub>V</sub>" [4]. The types of cavitation tribosystem, according to the action of water upon the fixed triboelement, are presented in figure 1.

It is possible to confirm that the cooling systems, of the internal combustion engines, taking into account the triboelements (fixed at the cylinder block and mobile at cylinder liner), the interposed medium between triboelements (cooling fluid) and the nature of the mobile triboelement motion, is a vibration cavitation tribosystem, "T<sub>V</sub>". Also, as a consequence of the liquid jet impact, the cavitation in the input-output cooling water sections develops. Our experiment shows that vibration cavitation is predominant.

In figure 2 the structure of a tribosystem is presented. It contains three groups of components:

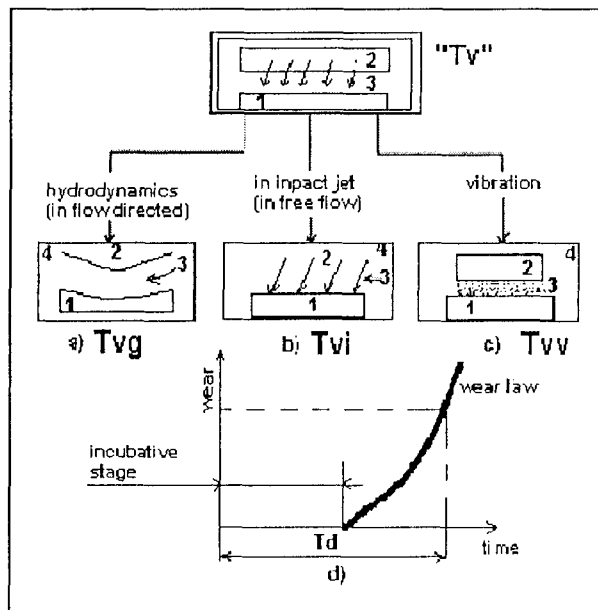


Figure 1. Cavitation tribosystem. Wear law

1. The input - output components: the parameters of superficial layer, "S<sub>s</sub>", (microgeometry, hardness, tension state, structure, chemical composition, purity) and the characteristic parameters of the tribosystem, "C<sub>r</sub>", (diameter, material and cylinder liner thickness).
2. The command components, "U": the constructive, the medium parameters and the exploitation parameters.
3. The components for the estimation of the wear effects: noise level, vibrations, thermal level.

C. Gheorghies, M. Simionov  
Dunarea de Jos" University of Galati, Romania

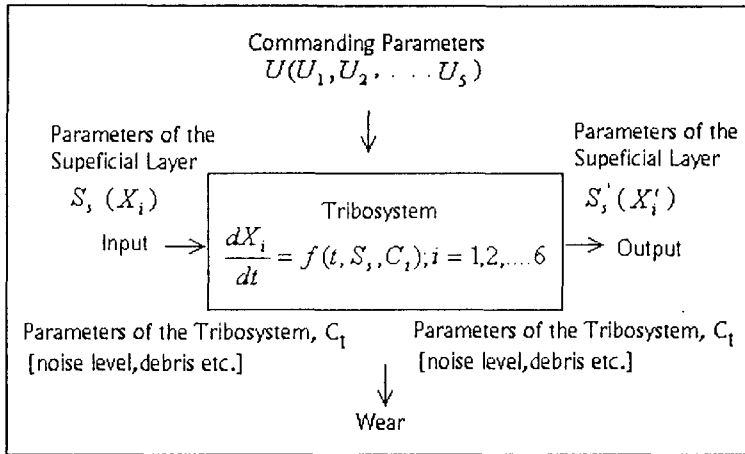


Figure 2. The structure of a tribosystem

## 2. WORKING METHODOLOGY

With a view to the cavitation wear study of the Diesel engines cylinder liners from a special stand has been realised. A large report is given in paper [4]. In order to analyse the tribomodel input-output values, a vibration regime of the cylinder liner has been selected at bigger values than the values determined on the engine [5].

The level of the second order inner tension in martensite phase has been evinced by the X-ray diffraction method using the diffraction line width, B220. It is known that the diffraction line width, B220, is directly proportional to the second order inner tension [6]. The distribution of the X-ray diffraction measurement points is presented in figure 3.

The vibrations are exerted on the direction of the symmetry axis 5-1 upon the internal surface of the cylinder liner, (figure 3). The binding conditions of the cylinder liner in the superior and inferior guides are the same on the entire circumference. It is possible to appreciate that the second order inner tensions induced in the superficial layer are disposed symmetrically with the axis 5-1.

The diffraction line width, B<sub>220</sub>, has been measured at the interval of 25 hours, during vibration tests. By means of the X-ray diffractometer, the measurements concerning the evolutions of the dislocation density " $\rho$ ", in the crystal lattice of the superficial layer of the cylinder liner

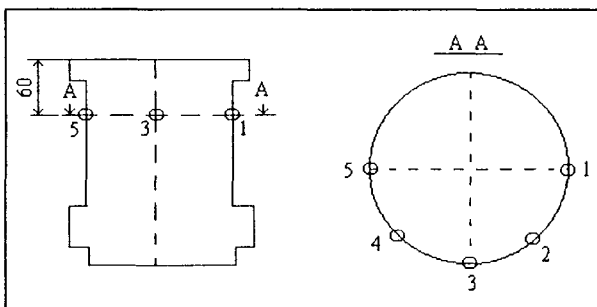


Figure 3. The distribution of measurement points

were realised. In the X-ray diffraction spectrum, the diffraction line (220) was selected and the values  $I_{bg}$  (background intensity) and  $I_{max}$  (maximum intensity) were estimated. The ratio  $I_{bg}/I_{max}$  is proportionally to  $\rho$ .

The cylinder liners are manufactured by the antifriction grey cast-iron with lamelle graphite. The chemical composition of the cast iron used was: C - (3.2 - 3.5)%; Si - (1.9 - 2.2)%; Mn - (0.6 - 0.9)%; S - max 0.12%; Cr - (0.25 - 0.60)%; Cu - (0.4 - 0.8)%; P - (0.4 - 0.6)%; Ni - (0.01 - 0.12)%; Mo - (0.05 - 0.12)%; V - (0.01 - 0.02)%.

## 3. EXPERIMENTAL RESULTS

For the cylinder liner of 6 mm and 4 mm in thickness, the dependencies of the diffraction line width versus testing time are presented in figures 4 and 5.

For the cylinder liner of 6 mm, we conclude that: a) in the points 1 and 5, the tension variation is monotonously decreasing (releasing process in point 1) and, respectively, monotonously increasing (tension process in point 5), the release amplitude being smaller than the tension amplitude; b) in the points 2, 3 and 4, the tension variation is oscillatory, a fact that can be associated with a fatigue process [7].

For the cylinder liner of 4 mm thickness, we conclude that: a) in the point 1, the inner second order tension variation is jumping, being characterised by bigger amplitude and period; this can be associated with a fatigue process; b) in the point 2, the tension curve is characteristic for the slow fatigue process, taking into account the small amplitude tension-release processes of the crystalline lattice; c) in the points 3 and 5 the release processes occur, being more powerful in 3 and slower in 5; d) in the point 4 a fatigue process with release tendency is manifesting; e) all the fatigue processes develop under the initial level of the inner second order tension.

In figure 6 and 7, the epires of the inner second order tensions, for 6mm. and 4 mm thickness, respectively, are presented. They give a general image on the distribution and evolution of the tension states in the mosaic blocks.

For the cylinder liner of 6 mm and 4 mm in thickness, the dependencies of the ratio  $I_{bg}/I_{max}$  versus testing time, in the figures 8 and 9, respectively, are presented.

In the case of the thinner material (4 mm), the damage process occurs due to the fatigue of crystalline lattice. The fatigue process is generated both the mechanical

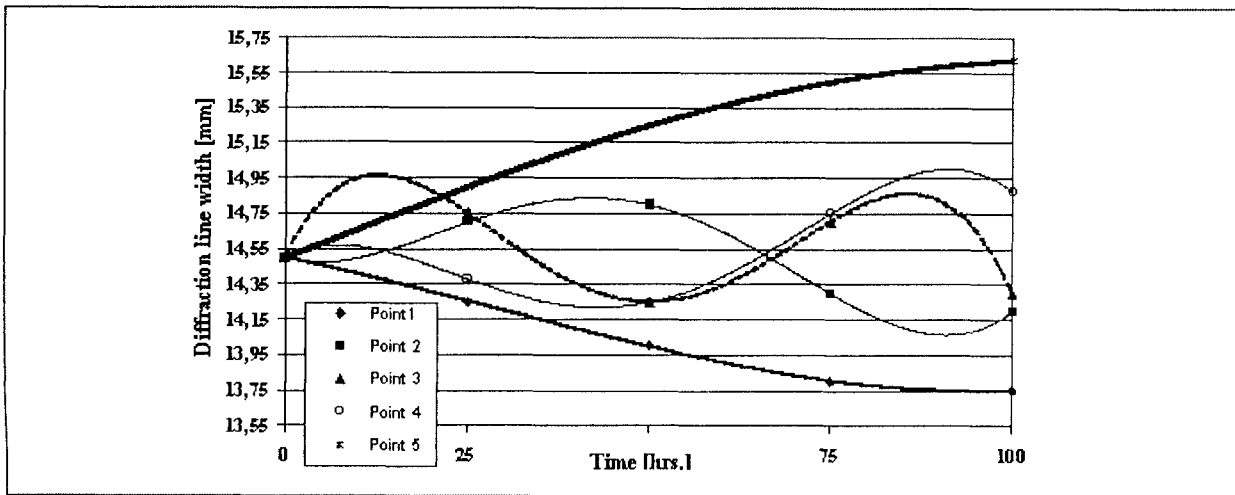


Figure 4. Dependence of inner second order tension versus testing time (Thickness = 6 mm)

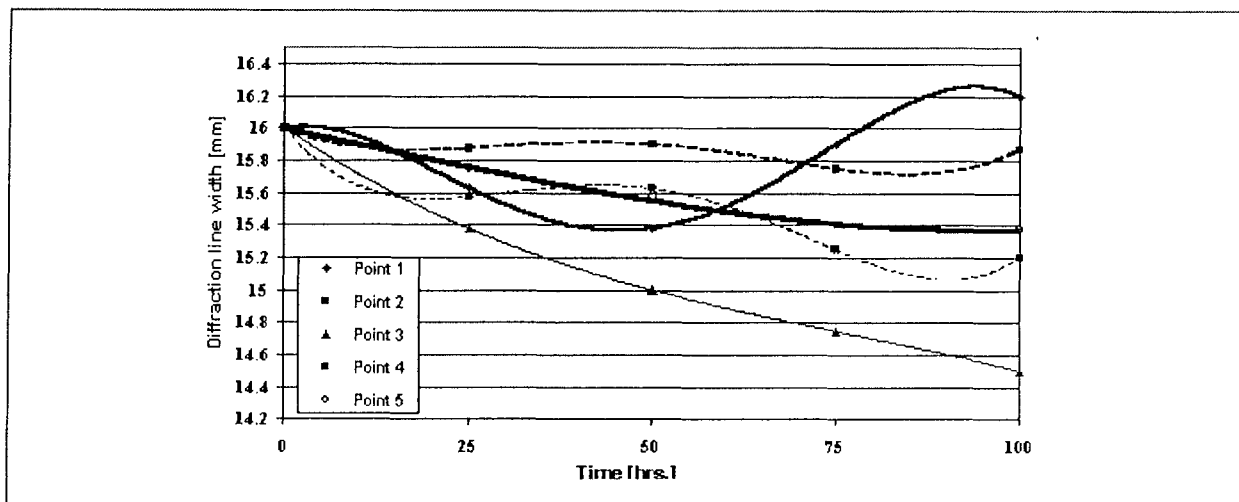


Figure 4. Dependence of inner second order tension versus testing time (Thickness = 4 mm)

vibration and collapsing of gas bubbles on the external surface of the cylinder liner during cavitation test.

The epures of the dislocation density, for 6mm and 4 mm in thickness, respectively, in figures 10 and 11 are presented. They also give a general image on the distribution and evolution of the dislocations during testing process.

In the case of the thicker material (6 mm), the evolution of the dislocation density during cavitation test allows to conclude that the damage process of the superficial layer begins with an accumulation and blocking of the dislocations at various obstacles in the crystalline lattice. This fact allows the appearance of the microcracks, which by their addition, lead to a major crack.

In figure 12, the epures of microhardness after 100 hrs. testing time are displayed. In figures 13 and 14 the distribution of the microhardness in the superficial layer on semicircle for the two thicknesses are presented. For both thicknesses, the result is that the value of the microhardness decreases, is more pronounced in points 1 and

5. This is in relationship with the damage level by cavitation wear.

In figure 15, the dependence of the roughness, in different measurement point, versus testing time is presented. This distribution shows a high reduction of the roughness due to a strong collapse of the air bulbs at the surface that cuts the tops of the material.

In figure 16 the dependence of the lost material on testing time, in two regimes, is presented. This loss is determined by the cavitation process, chemical corrosion and cooling water circulation regime. These processes are influenced by temperature, the wear taking a maximum value for a temperature of 60°C.

After a testing time of 100hrs., the microstructure in point 3 of the cylinder liner of 6 mm in thickness was studied. This microstructure with and without a chemical attack in figures 17 and 18 respectively is presented. In the photos the graphite lamellae and the misses are visible.

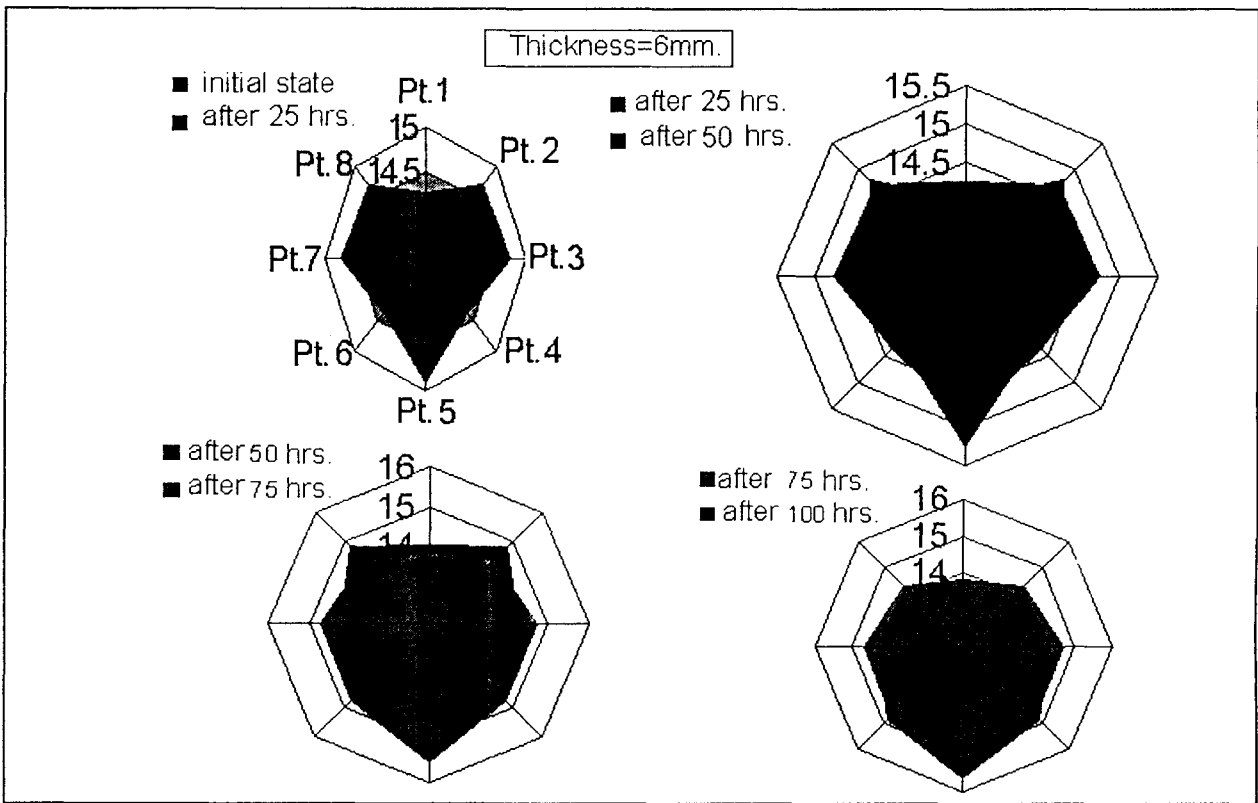


Figure 6. Epure of the tension state after 25, 50, 75 and 100 hrs. testing time

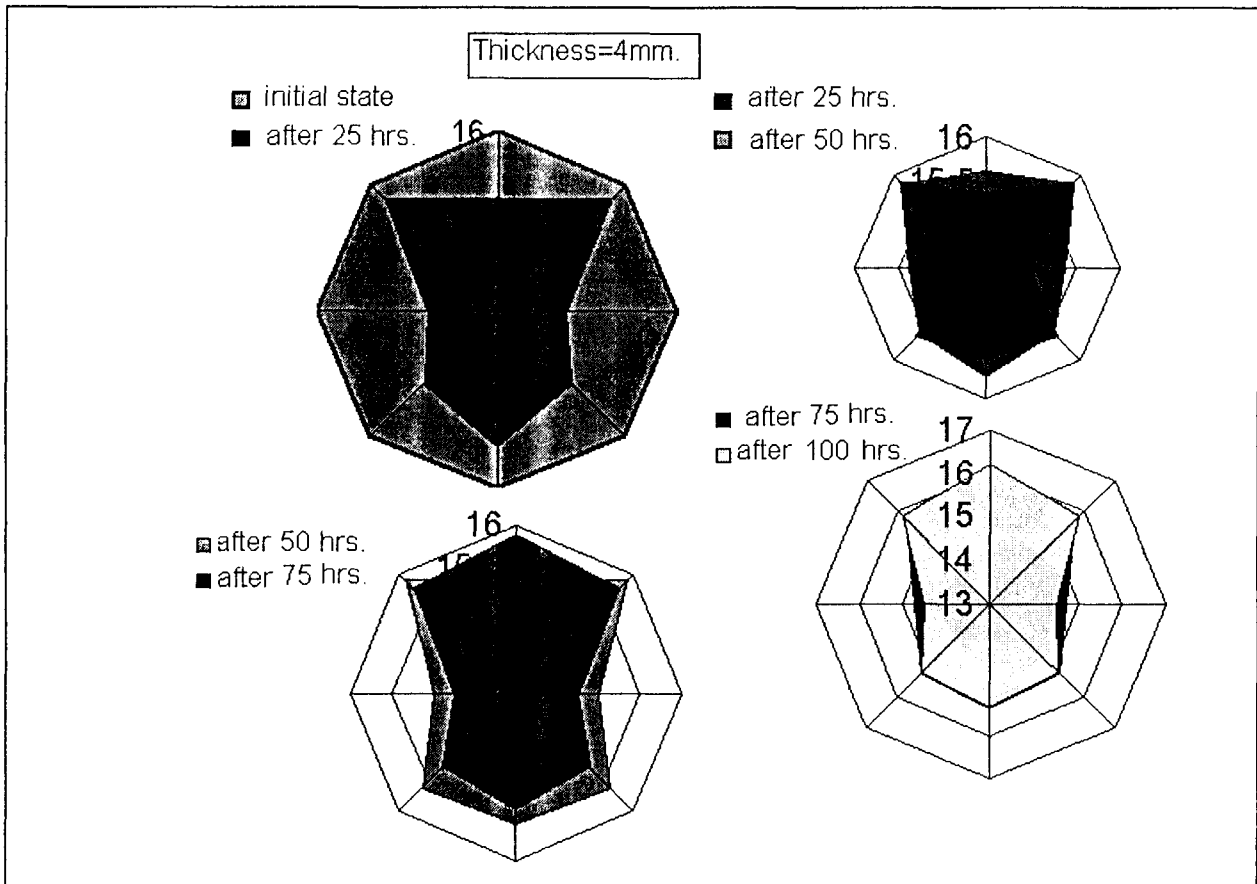


Figure 7. Epure of the tension state after 25, 50, 75 and 100 hrs. testing time

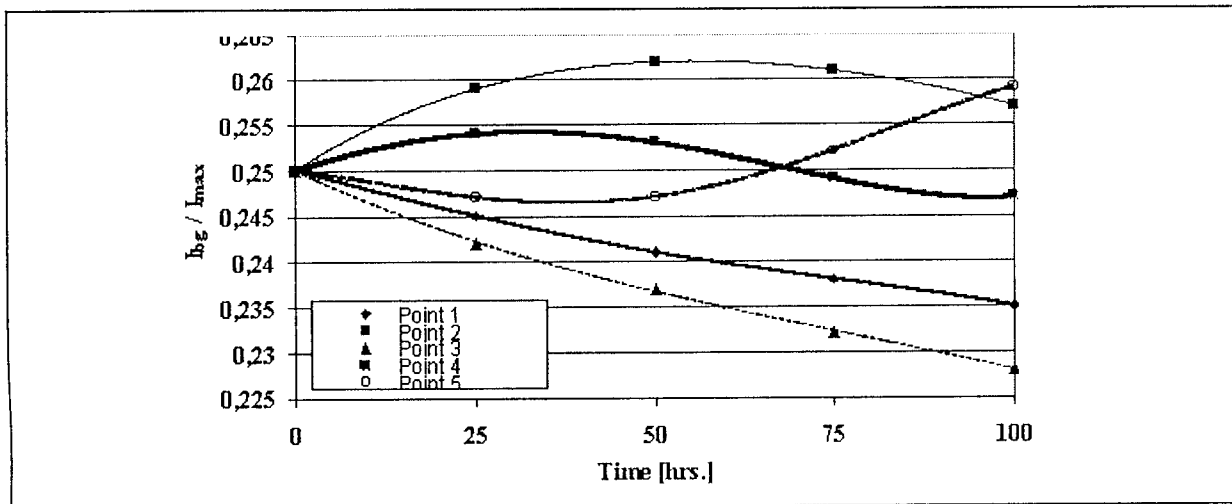


Figure 8. Dependence of dislocation density versus testing time (Thickness = 6 mm)

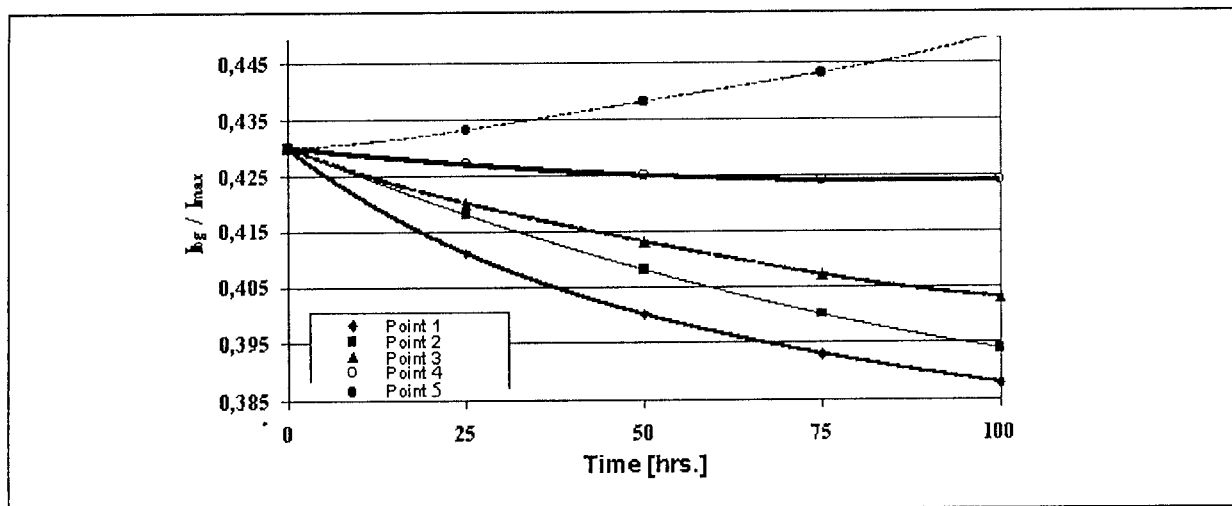


Figure 9. Dependence of dislocation density versus testing time (Thickness = 4 mm)

These misses are small and the cracks appear near graphite lamellae. Also, the grain structure of the surface layer after damage process by cavitation was evinced using optical microscopy method. In this aim, the samples were taken from the regions where the structural changes have been checked by X-ray diffraction method. The obtained images evinced that there is a lot of dislocated graphite lamella.

Our results have been applied in the study of the Diesel engine cylinder liner during working process.

#### 4. CONCLUSIONS

In the surface layer of the cylinder liner, during the vibration process, some structural changes develop, which lead to its damage.

The researches showed that:

1. The variation of the inner second order tensions in the surface layer is given both the mechanical vibra-

tions of the cylinder liner and the cavitation bubble breaking on its surface.

2. The variation curves of the inner second order tensions are typical of a fatigue process, monotonously decreasing (release process) and monotonously increasing (tension process).
3. From the variation of the dislocations density and the inner second order tension, we can conclude that, in the case of the cylinder liners of 4 mm thickness, the damage process has at its basis a fatigue process of the crystalline lattice, given by the evolution in jumps of the second order inner tensions at the superior zone of the cylinder liner.
4. In the case of the cylinder liner of 6 mm in thickness, the dislocation density evolution, corroborated with the inner second order tension evolution, lead to the conclusion that the beginning of the damage process is a consequence of the agglomeration and blocking of dislocations in different barriers and it is possible

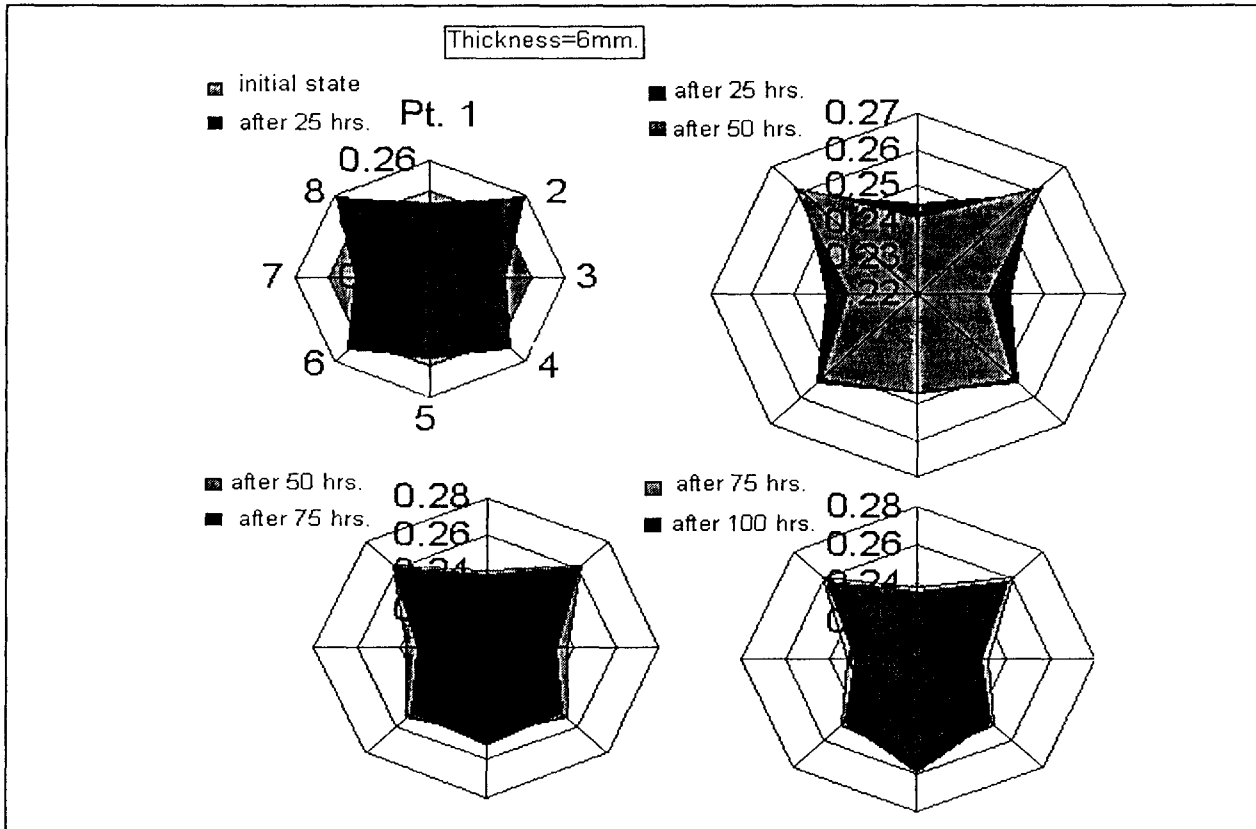


Figure 10. The epure of dislocation density after 25, 50, 75 and 100hrs. testing time

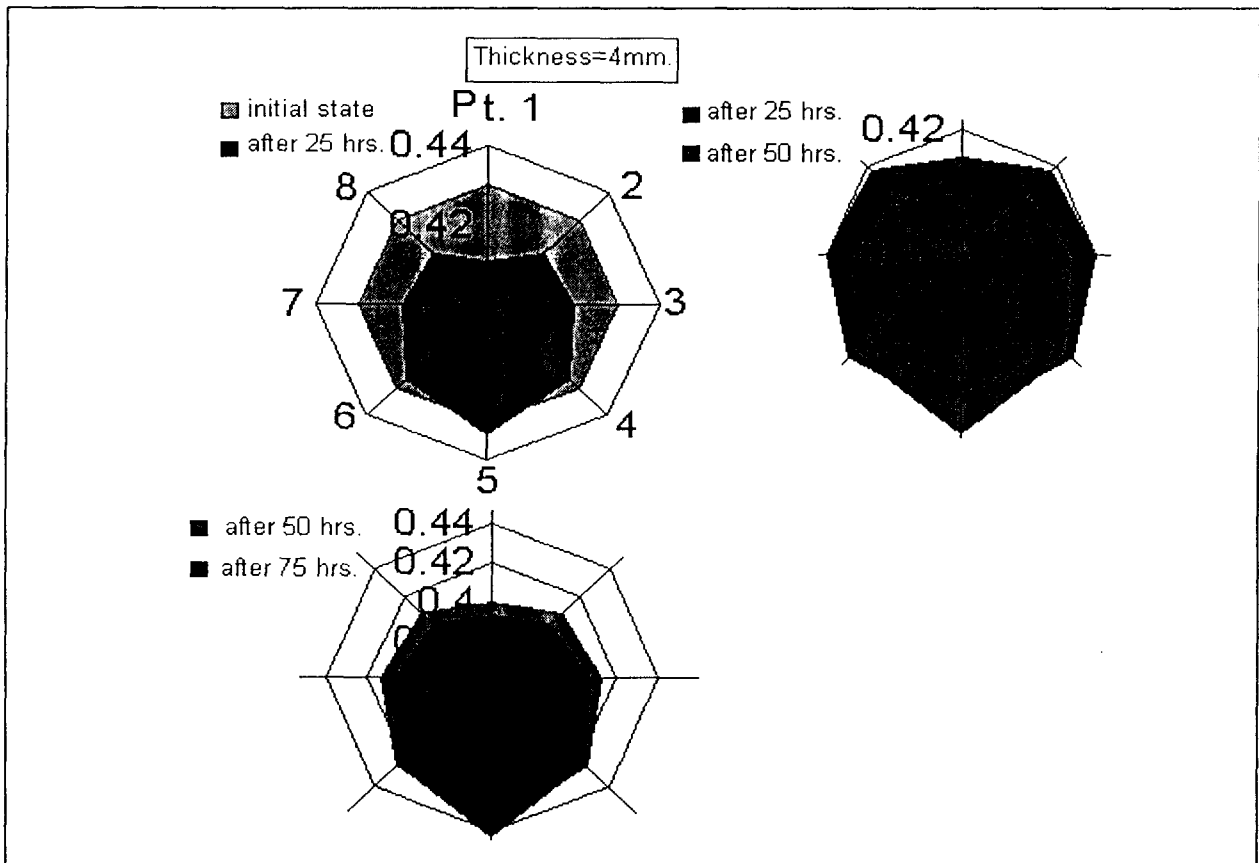


Figure 11. The epure of dislocation density after 25, 50, 75 and 100hrs. testing time

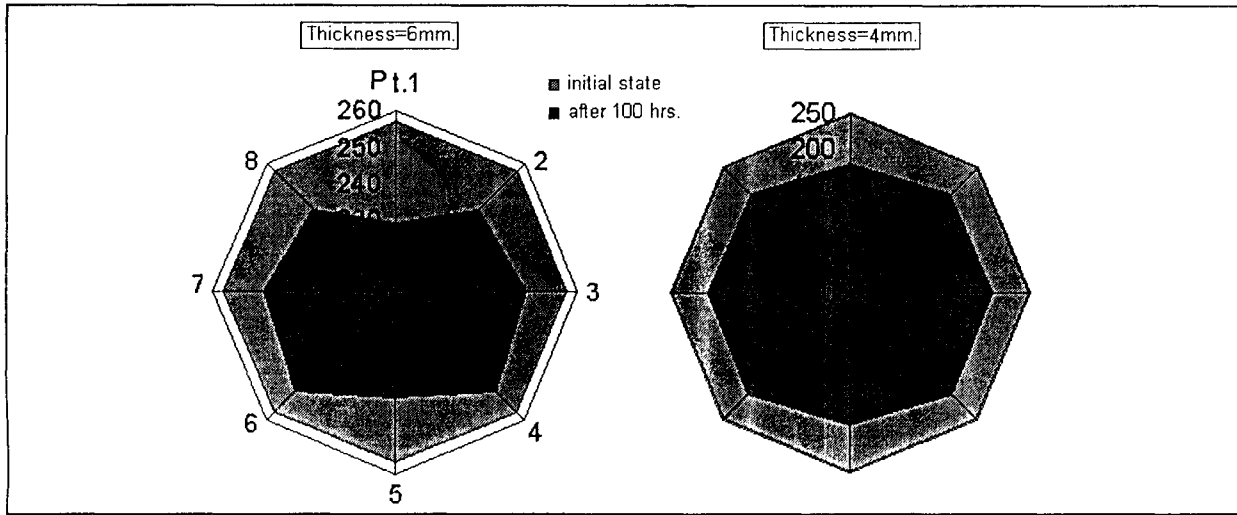


Figure 12. The epure of the microhardness in the surface layer

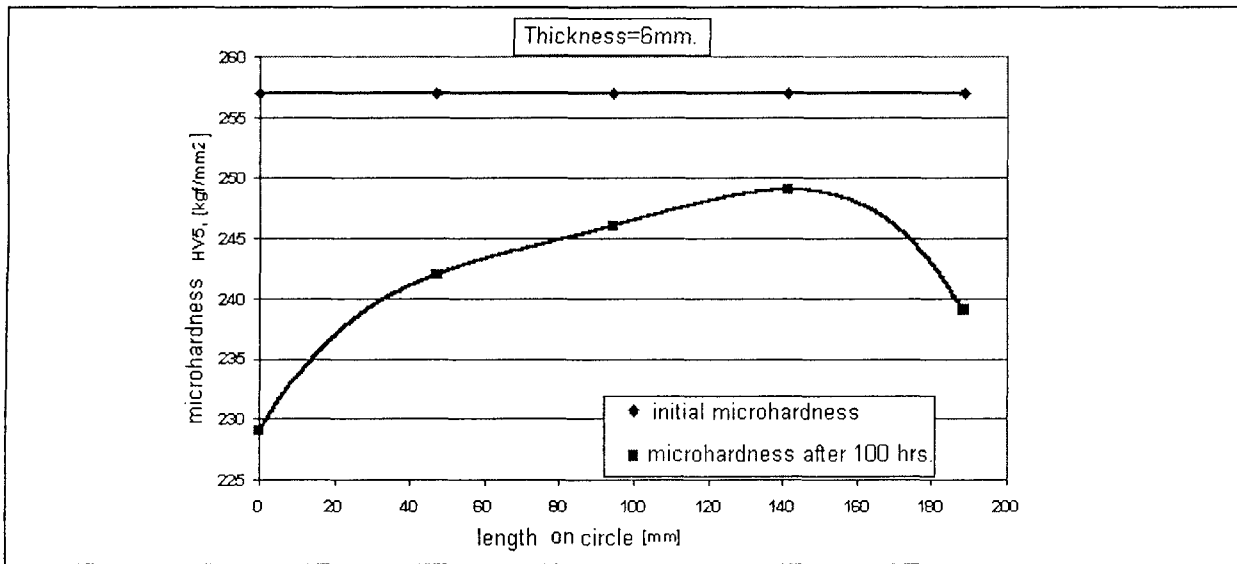


Figure 13. The dependence of the microhardness versus length on semicircle

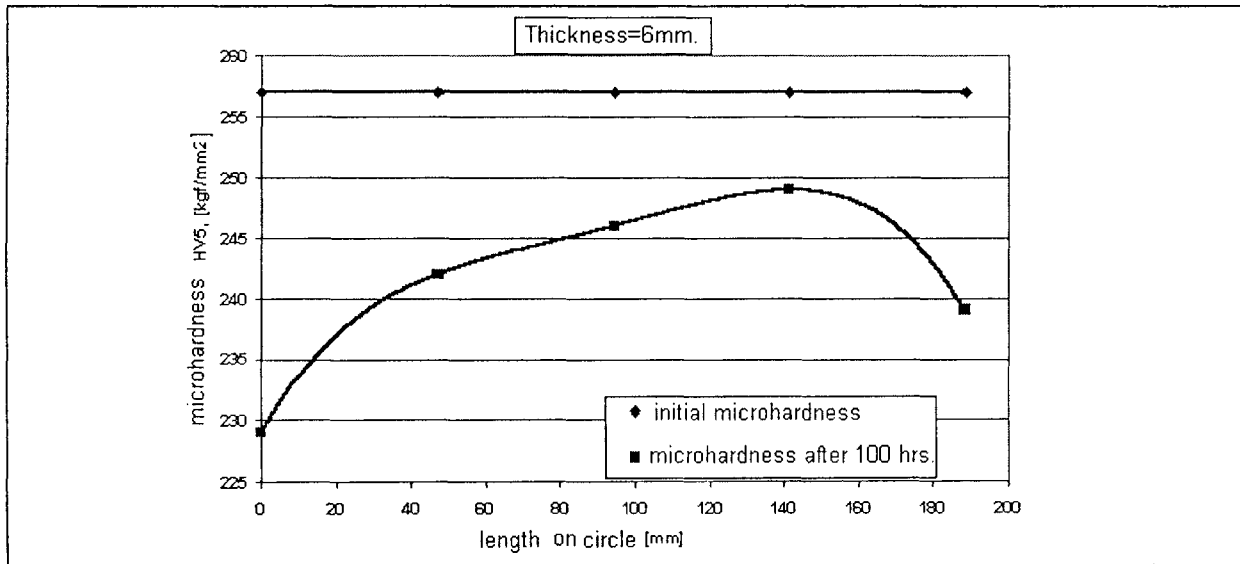


Figure 14. The dependence of the microhardness versus length on semicircle

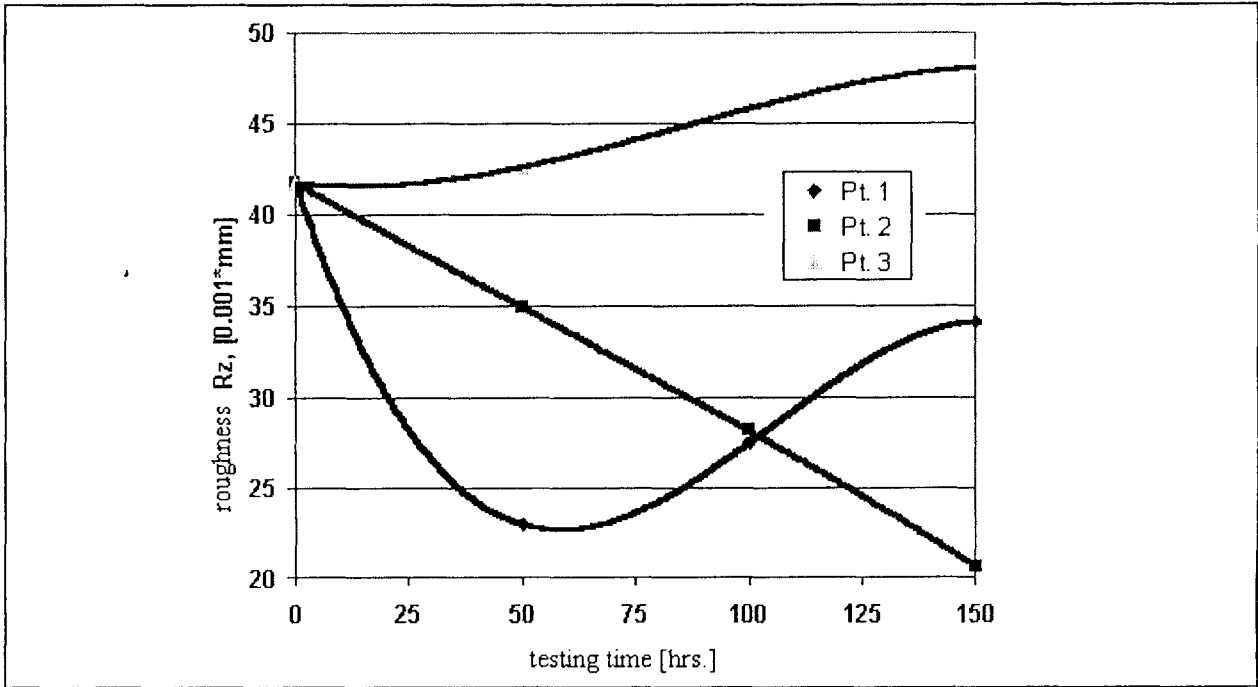


Figure 15. The dependence of the roughness on testing time

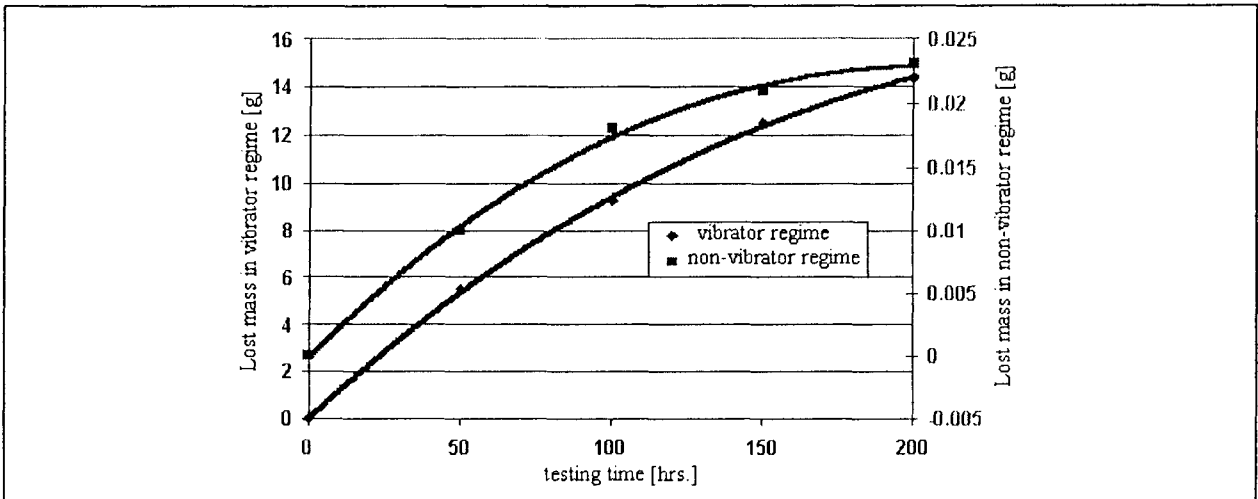


Figure 16. The dependence of lost mass versus testing time



Figure 17. Microstructure and lamella graphite, before chemical attack

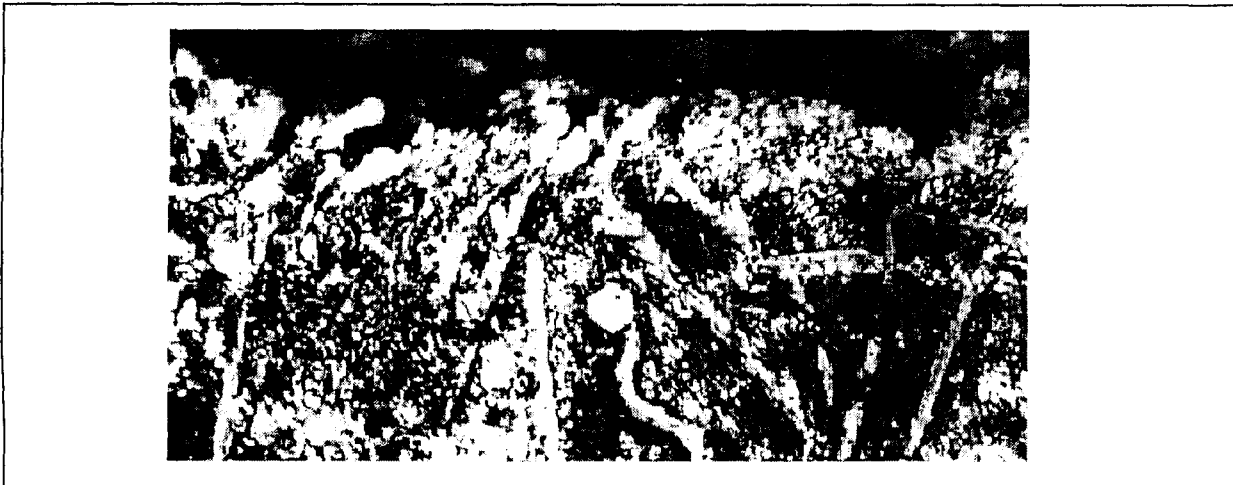


Figure 18. Microstructure and a graphite lamellae, after chemical attack

to appear in the zone of the cylinder liner where the vibrations are maximum.

5. The study on the tribomodel allowed to establish the time-evolution during vibration process of some surface layer parameters as: inner second order tensions and dislocations density. These evolutions can be used to explain the damage by cavitation process of a polycrystalline surface layer in a cylinder liner of Diesel engines.

#### REFERENCES

- [1] *Simionov M., Ph. D. Thesis, University "Dunarea de Jos" of Galati, Romania, 1997*
- [2] *Gheorghies C., Gheorghies O., Prediction of case-hardening steel behaviour in rolling tribosystem, Tribology in Industry, vol.20,1, March, 1998, p.5*
- [3] *Crudu, I., Palaghian, L., Gheorghies, C. : Proc. of the Japan International Tribology Conference, Nagoya, Japan, 1990, p. 209.*
- [4] *Crudu, I., Simionov, M., Gheorghies, C. Proc. of the 8th Int. Conf. on Trib., NORDTRIB'98, Ebeltoft, Denmark, vol. I, 1998, p. 183.*
- [5] *Gheorghies, C. Structural Changes During Friction, Wear and Fatigue Processes (in Romanian), Technical Publishing House, Bucuresti, Romania, 1997*
- [6] *Gheorghies, C. Proc. of the 16th CMD, Leuven, Belgium, 1997, p.169*
- [7] *Bersadskii, L. I., O voizvoistnosti struktunih mehanizmov i dissipativnih potokov prin kineticeskom trenie i iznose, Trenie i Iznos no.2, 1989*
- [8] *Josifovic D., Markovic S, Proc. of The BALKANTRIB'99, Sinaia, Romania, vol.III, p.381*